The Journal of Immunology

Protective Role of Macrophages in Noninflammatory Lung Injury Caused by Selective Ablation of Alveolar Epithelial Type II Cells[1]

Yasunobu Miyake,* Hitomi Kaise,* Kyo-ichi Isono,† Haruhiko Koseki,† Kenji Kohno,‡ and Masato Tanaka[2]*

Macrophages have a wide variety of activities and it is largely unknown how the diverse phenotypes of macrophages contribute to pathological conditions in the different types of tissue injury in vivo. In this study we established a novel animal model of acute respiratory distress syndrome caused by the dysfunction of alveolar epithelial type II (AE2) cells and examined the roles of alveolar macrophages in the acute lung injury. The human diphtheria toxin (DT) receptor (DTR), heparin-binding epidermal growth factor-like growth factor (HB-EGF), was expressed under the control of the *lysozyme M* (*LysM*) gene promoter in the mice. When DT was administrated to the mice they suffered from acute lung injury and died within 4 days. Immunohistochemical examination revealed that AE2 cells as well as alveolar macrophages were deleted via apoptosis in the mice treated with DT. Consistent with the deletion of AE2 cells, the amount of surfactant proteins in bronchoalveolar lavage fluid was greatly reduced in the DT-treated transgenic mice. When bone marrow from wild-type mice was transplanted into irradiated LysM-DTR mice, the alveolar macrophages became resistant to DT but the mice still suffered from acute lung injury by DT administration. Compared with the mice in which both AE2 cells and macrophages were deleted by DT administration, the DT-treated LysM-DTR mice with DT-resistant macrophages showed less severe lung injury with a reduced amount of hepatocyte growth factor in bronchoalveolar lavage fluid. These results indicate that macrophages play a protective role in noninflammatory lung injury caused by the selective ablation of AE2 cells. *The Journal of Immunology,* 2007, 178: 5001–5009.

Macrophages exhibit a variety of activities including induction of inflammation, engulfment of microorganisms and dead cells, Ag presentation, and regulation of extracellular components (1–3). Consistent with these activities, macrophages play diverse roles at the site of tissue injury. At the site of bacterial infection, macrophages recognize invading microorganisms via a wide variety of surface receptors that bind the cellular components common to many bacterial surfaces, thereby engulfing them for elimination. Macrophages encountering bacteria also produce and secrete inflammatory cytokines and chemokines such as TNF-α, IL-6, and MIP-1α. These factors induce inflammation, and the inflammatory responses play a critical role in the effective clearance of invading bacteria and the induction of appropriate adaptive immunity. The inflammatory responses, however, can cause deleterious injury to local tissues.

In contrast, at the site of tissue injury macrophages also recognize cell debris and dead cells (4–6). Tissue injury and inflammation results in the death of resident stromal and parenchymal cells. In addition, infiltrating neutrophils are eliminated by apoptotic cell death during the late course of inflammation. Macrophages rapidly phagocytose these dead cell corpses by means of specific phagocytic receptors for dying cells. The clearance of dead cells prevents the release of potentially toxic or immunogenic intracellular materials from a dead cell corpse. Thus, the prompt elimination of dying neutrophils and damaged resident cells is required for the resolution of inflammation and normal tissue repair (7, 8). Apoptotic cell clearance by macrophages is associated with active immunosuppression by the production of such anti-inflammatory cytokines as TGF-β and IL-10 (9–11). This suppressive effect of macrophages in association with the clearance of dead cells may contribute to normal tissue repair. Thus, macrophages have both proinflammatory and anti-inflammatory phenotypes. However, these phenotypes have been defined predominantly in the in vitro culture of macrophages and it is largely unknown how these diverse phenotypes of macrophages contribute to pathological conditions in the different types of tissue injury in vivo.

To study the effects of loss of a specific cell type in animal models, several approaches have been attempted for inducible cell-specific ablation. Recently, Saito et al. (12) reported a method for conditional cell ablation called TRECK (toxin receptor-mediated cell knockout) that works by expressing the human diphtheria toxin (DT)[3] receptor (DTR) in transgenic mice. Human heparin-binding epidermal growth factor-like growth factor (HB-EGF) acts

---

*Laboratory for Innate Cellular Immunity, and †Developmental Genetics Group, RIKEN Research Center for Allergy and Immunology, Yokohama, Japan; and ‡Graduate School of Biological Sciences, Nara Institute of Science and Technology, Ikoma, Japan

Received for publication December 29, 2006. Accepted for publication January 30, 2007.

The costs of publication of this article were defrayed in part by the payment of page charges. This article must therefore be hereby marked *advertisement* in accordance with 18 U.S.C. Section 1734 solely to indicate this fact.

[1] This work was supported in a part by a Grant-in-Aid from the Ministry of Education, Culture, Sports, Science and Technology in Japan, the Uehara Foundation, and the Mochida Memorial Foundation for Medical and Pharmaceutical Research.

[2] Address correspondence and reprint requests to Dr. Masato Tanaka, Laboratory for Innate Cellular Immunity, RIKEN Research Center for Allergy and Immunology, 1-7-22 Suehiro, Tsurumi, Yokohama, Kanagawa, Japan. E-mail address: mtanaka@rcai.riken.jp

[3] Abbreviations used in this paper: DT, diphtheria toxin; AE1, alveolar epithelial type I; AE2, alveolar epithelial type II; ARDS, acute respiratory distress syndrome; BALF, bronchoalveolar lavage fluid; DIG, digoxygenin; DTR, DT receptor; ES, embryonic stem; FasL, Fas ligand; HB-EGF, heparin-binding epidermal growth factor-like growth factor; HGF, hepatocyte growth factor; LysM, lysozyme M; SP, surfactant protein.

Copyright © 2007 by The American Association of Immunologists, Inc. 0022-1767/07/$2.00

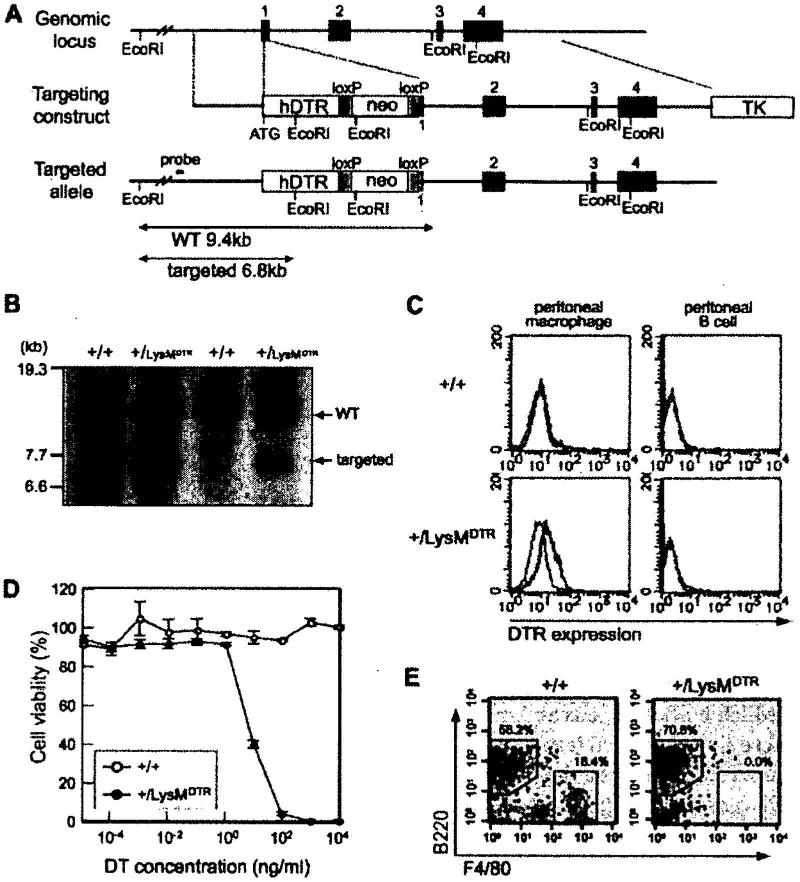

FIGURE 1. Targeting strategy for the introduction of human *DTR* into the *LysM* gene. *A*, Schematic diagram of the LysM-DTR targeting construct. Exons 1 through 4 of the *LysM* gene are indicated by solid boxes. In the targeting construct, human diphtheria toxin receptor (hDTR) cDNA, the *loxP*-flanked neomycin resistance gene (neo) cassette, and the thymidine kinase (TK) cassette are indicated by boxes. The probe used for Southern blot analysis is indicated as a solid line together with the predicted hybridizing fragments. WT, wild type. *B*, Genomic Southern blot analysis of LysM-DTR mice using an *Eco*RI digest in combination with the indicated probe. WT, wild type. *C*, Surface expression of human DTR protein on peritoneal macrophages from LysM-DTR mice. Peritoneal cells were prepared from wild-type (+/+) or LysM-DTR (+/LysM^{DTR}) mice. Macrophages and B cells were stained with anti-DTR mAb and analyzed with a flow cytometer. Black and green lines indicate no staining and anti-DTR staining, respectively. *D*, Sensitivity of macrophages to DT ex vivo. Thioglycollate-elicited peritoneal macrophages were prepared from wild-type (+/+) or LysM-DTR (+/LysM^{DTR}) mice and cultured overnight. The cells were then treated with the indicated concentrations of DT for 20 h. Cell viability was measured using a colorimetric reagent, WST-8. The assay was performed in triplicate and average values are shown with the SD. *E*, Inducible ablation of peritoneal macrophages by DT administration to LysM-DTR mice. DT at 40 μg/kg was injected i.p. into wild-type (+/+) or LysM-DTR (+/LysM^{DTR}) mice. Forty-eight hours later, peritoneal cells were prepared from these mice and stained with anti-F4/80 and anti-B220 Abs for macrophages and B cells, respectively.

as a DTR, whereas mouse HB-EGF possesses negligible affinity to DT. Thus, mouse cells are more resistant to DT than human cells (13–15). When the human *HB-EGF* gene is transduced into mice under the control of a cell-specific promoter, the target cells are transiently depleted by DT administration in vivo (12, 16). This technique allows us to achieve efficient inducible ablation of a specific cell type by the administration of DT to the mice.

In this study we have developed a line of transgenic mice expressing human DTR under the control of the *lysozyme M* (*LysM*) gene promoter. Our initial goal was to induce ablation of various macrophages in vivo. However, in addition to macrophages the alveolar epithelial type II (AE2) cells in the lung were killed by administration of DT, and the mice suffered from acute respiratory failure in association with the lack of surfactant proteins (SPs). We also generated conditional AE2 ablation with or without the ablation of macrophages by means of bone marrow transplantation. The analysis of these mice revealed that macrophages play a protective role in noninflammatory lung injury caused by the selective ablation of AE2 cells.

Materials and Methods

Targeting vector construction and generation of LysM-DTR mice

A genomic clone containing the *LysM* gene was obtained from a BAC library of 129/Sv mouse genomic DNA (Research Genetics). To generate the targeting vector, the region from −1.6 to +6.6 kbp relative to the transcriptional start site of the *LysM* gene was subcloned into pBluescript II SK(+) vector (Stratagene). Then, a 115-bp fragment in exon 1 was replaced with human *DTR* (*HB-EGF*) cDNA with a polyadenylated tail by a recombinant PCR technique. To select for homologous recombinants, a *loxP*-flanked Neo cassette was cloned downstream of the human *DTR* gene. The thymidine kinase gene was inserted downstream of the 3′ arm to select against random integrants. The final targeting vector was linearized with *Pvu*I for transfection.

To generate LysM-DTR mice, R1 embryonic stem (ES) cells were transfected with the targeting vector by electroporation. G-418- and gancyclovir-resistant clones were screened for homologous recombination by Southern blot analysis. Germline chimeric mice were generated by aggregation methods (17). Chimeric mice with a high ES cell contribution were crossed with C57BL/6 mice to produce +/LysM^{DTR} mice. +/LysM^{DTR} mice were backcrossed to C57BL/6 mice three to six times, and the wild-type (+/+) and heterozygous LysM-DTR (+/LysM^{DTR}) littermates were used for analysis. All mice were housed in a specific pathogen-free facility. Experiments were performed according to institutional guidelines.

For Southern blot analysis, genomic DNA was prepared from a mouse tail biopsy as described previously (18). For Southern hybridization, genomic DNA was digested with *Eco*RI, separated by electrophoresis on a 0.8% agarose gel, and transferred to a Biodyne A membrane (Pall). Hybridization was conducted with a 200-bp digoxygenin-labeled DNA fragment located outside the targeting vector according to the recommended protocols (DIG System for Filter Hybridization; Roche).

Antibodies

Anti-human DTR mAb was prepared by immunizing Armenian hamsters with human DTR-expressing cells. In brief, a DNA fragment for the full-length coding sequence of human *DTR* from pMS7 vector (12) was subcloned into the pEF-BOS-EX vector (19). The expression plasmid was introduced into human 293T cells by the calcium phosphate precipitation method. Beginning 24 h later, human DTR-expressing cells (1.5 × 10^7 cells) were injected s.c. into hamsters four times with 1-wk intervals between injections. A final booster was performed by injecting 1 × 10^7 cells of human DTR-expressing cells into the footpads. Three days after the final boost, the hamster was sacrificed and lymphocytes were harvested from the lymph nodes and fused with NSO^{bcl-2} mouse myeloma cells (20). Hybridomas were tested by ELISA with human DTR-expressing cells and three clones for anti-human DTR Ab were obtained. The hybridomas were cultured in GIT medium (Nihon Seiyaku) and Ab was purified by protein A-Sepharose 4FF beads (Amersham Biosciences). Fluorescent labeling of

Ab was performed using an Alexa Fluor 488 mAb labeling kit (Molecular Probes).

Anti-FcγIII/II receptor Ab (clone 2.4G2), PE-anti-CD11b Ab (clone M1/70), and PE-anti-B220 Ab (clone RA3-6B2) were obtained from BD Biosciences. Anti-SP-A, -B, and -D Abs were obtained from Chemicon International. Anti-TTF-1 Ab (clone 8G7G3/1) and HRP-labeled anti-mouse Ig and anti-rabbit Ig Abs were obtained from DakoCytomation. Anti-T1α Ab (clone 8.1.1) was obtained from the Developmental Studies Hybridoma Bank (University of Iowa, Iowa City, IA). Anti-CD169 Ab (clone 3d6.112) was obtained from Serotec. Cy3-labeled anti-rat IgG Ab and HRP-labeled anti-hamster IgG Ab were obtained from Jackson ImmunoResearch Laboratories. Biotinylated anti-F4/80 Ab (clone CI:A3-1) was obtained from Caltag Laboratories. Anti-F4/80 Ab (clone 6-16A; M. Tanaka and S. Nagata, unpublished observations) was provided by Dr. S. Nagata (Osaka University, Osaka, Japan). Fluorescein-anti-DIG Ab was obtained from Roche.

Ex vivo cytotoxic assay

Thioglycollate-elicited peritoneal macrophages (1×10^5 cells) were cultured in DMEM containing 10% FCS overnight. DT was added to macrophage culture and incubated for 20 h and then cell viability was measured by Cell Counting Kit-8 (Dojindo Laboratories).

FACS analysis

Mouse peritoneal elicited cells (1×10^5 cells) were preincubated with anti-FcγIII/II receptor Ab and were stained with biotinylated anti-F4/80 Ab (clone 6-16A). Cells were then washed, incubated with PE-anti-B220 or PE-CD11b Abs and streptavidin-Alexa Fluor 488 (Molecular Probes), and analyzed by a FACSCalibur system with the CellQuest program (BD Biosciences). To detect the DTR expression, cells were stained with an Alexa Fluor 488-labeled anti-DTR mAb (KM018).

Histology and immunohistochemistry

In all of the experiments except those with H&E staining the lungs were inflated with 4% paraformaldehyde and 4% sucrose in 0.1 M phosphate buffer (pH 7.2) through the trachea. For paraffin sections the lungs were immersion fixed in 4% paraformaldehyde in PBS overnight at 4°C and embedded in paraffin. For cryosections, the lungs were immersion fixed with 4% paraformaldehyde and 4% sucrose in 0.1 M phosphate buffer (pH 7.2) for 2 h at room temperature. Then, the lungs were washed with PBS, immersed in 10 and 20% sucrose in phosphate buffer, and embedded in Tissue-Tek OCT (Sakura).

Paraffin sections (5 μm) were mounted on coated slides (Matsunami adhesive slides; Matsunami Glass Industries) and stained with H&E. Apoptotic cells were detected by TUNEL staining using a peroxidase in situ apoptosis detection kit (Chemicon), followed by counterstaining with methyl green in paraffin sections.

For T1α and TTF-1 staining, paraffin sections were deparaffinized in xylene and rehydrated through a graded series of ethanol and then the slides were autoclaved for Ag retrieval. The sections were then quenched with 3% hydrogen peroxide in PBS, and blocked with 1.5% normal goat serum and 2% Block Ace (Snow Bland Milk Products). Slides were subsequently immunostained with anti-T1α Ab overnight at 4°C or an anti-TTF-1 Ab for 1 h at room temperature. Sections were washed and incubated for 1 h at room temperature with HRP-labeled anti-hamster IgG (for T1α) or anti-mouse Ig (for TTF-1). Signals were detected with a liquid diaminobenzidine substrate kit (Zymed Laboratories).

For F4/80, SP-A, -B, and -D staining, cryosections (4 μm) were mounted on 3-aminopropyltriethoxy silane-coated slides. Sections were fixed in cold acetone and blocked with 1.5% normal goat serum and 2% Block Ace. Slides were incubated with biotinylated anti-F4/80 Ab (Caltag Laboratories) for 1 h at room temperature or with anti-SP-A, -B, or -D Abs (Chemicon International) overnight at 4°C. The sections were then incubated with peroxidase-labeled streptavidin (Roche) for F4/80 or HRP-labeled anti-rabbit Ig Abs for SP-A, -B, and -D.

For double staining of TUNEL and CD169, 4-μm cryosections were first labeled with DIG-dUTP and blocked with 1.5% normal goat serum and 2% Block Ace. The sections were then incubated with anti-CD169 Ab followed by fluorescein-anti-DIG Ab and Cy3-anti-rat IgG Ab. The stained sections were mounted with FluorSave (Calbiochem) and observed by fluorescence microscopy (Olympus IX-71).

For transmission electron microscopy, the lungs were fixed with 2% glutaraldehyde in 0.1 M phosphate buffer (pH 7.2), washed with 0.14 M sucrose and 0.1 M phosphate buffer, postfixed with 1% OsO_4, 0.21 M sucrose, and 0.05 M phosphate buffer, and embedded in Epon 812. Sections (800~1000 Å) were prepared with U-5 Ultratome (LKB-BROMMA), stained with uranyl acetate and lead citrate, and observed with a JEOL 100S electron microscope (JEOL).

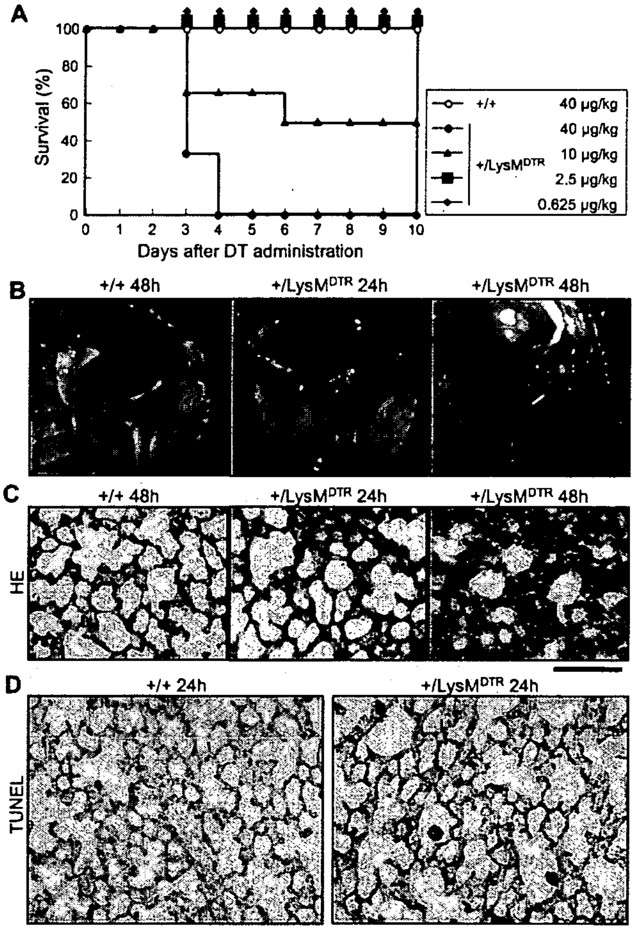

FIGURE 2. Lethal effect of DT administration on LysM-DTR mouse lung. *A*, The indicated amount of DT was i.p. injected into 6- to 8-wk-old wild-type (+/+) or LysM-DTR (+/LysM^{DTR}) mice. The number of mice in each group was 6–11 and the percentages of the mice that survived until the indicated time were plotted. *B–D*, DT at 40 μg/kg was i.p. injected into wild-type (+/+) or LysM-DTR (+/LysM^{DTR}) mice. Mice were sacrificed 24 or 48 h after DT administration. *B*, Macroscopic observation of the lung. *C* and *D*, Lungs were fixed with 4% paraformaldehyde and embedded in paraffin. The sections were stained with H&E (*C*) or TUNEL with methyl green staining (*D*). Scale bar, 100 μm.

Analysis of bronchoalveolar lavage fluid (BALF) and large aggregate

Mouse lungs were lavaged via tracheal cannula two times with 700-μl aliquots of PBS. Cell debris was removed by centrifugation at 200 × *g* for 10 min. For SP-B analysis, the large aggregate was separated from the BALF sample by centrifugation at 20,000 × *g* for 60 min and the pellet was resuspended in PBS.

For Western blot analysis, BALF samples and large aggregates were electrophoresed on polyacrylamide gels and then transferred to an Immobilon-P membrane (Millipore). Membranes were blocked in 5% skim milk in TBST before incubation with anti-SP-A, -B, and -D Abs. After washing, membranes were incubated with HRP-labeled anti-rabbit Ig Abs. Signals were detected using SuperSignal West Pico substrate (Pierce).

For cytokine ELISA, BALF was obtained from bone marrow chimeric mice after 24 h of DT treatment. The concentration of albumin and hepatocyte growth factor (HGF) in the BALF was measured by ELISA (Bethyl Laboratories and Institute of Immunology, Tokyo, Japan, respectively) according to the manufacturer's protocols.

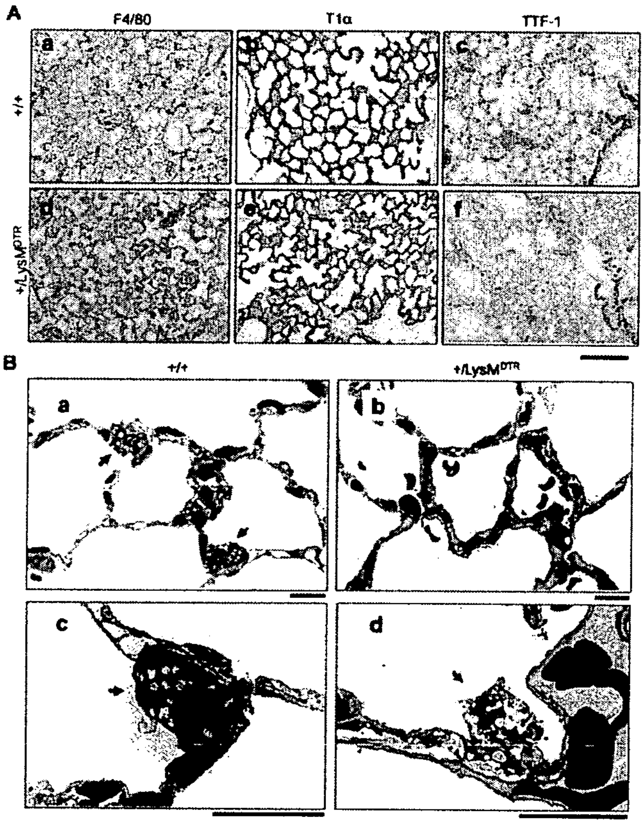

FIGURE 3. Effects of DT administration on alveolar macrophages and alveolar epithelial cells in lungs of LysM-DTR mice. Wild-type (+/+; *a–c*) or LysM-DTR (+/LysM^{DTR}; *d–f*) mice were i.p. injected with 40 μg/kg DT. Lungs were obtained from these mice 48 h after DT administration. *A*, The lung sections were immunostained with F4/80 (*a* and *d*), T1α (*b* and *e*), and TTF-1 (*c* and *f*), which are specific markers for alveolar macrophages, AE1, cells and AE2 cells, respectively. Scale bar, 100 μm. *B*, Transmission electron microscopic observation of the lung sections of wild-type (*a* and *c*) and LysM-DTR (*b* and *d*) mice. The red arrow indicates AE2 cells. Scale bar, 10 μm.

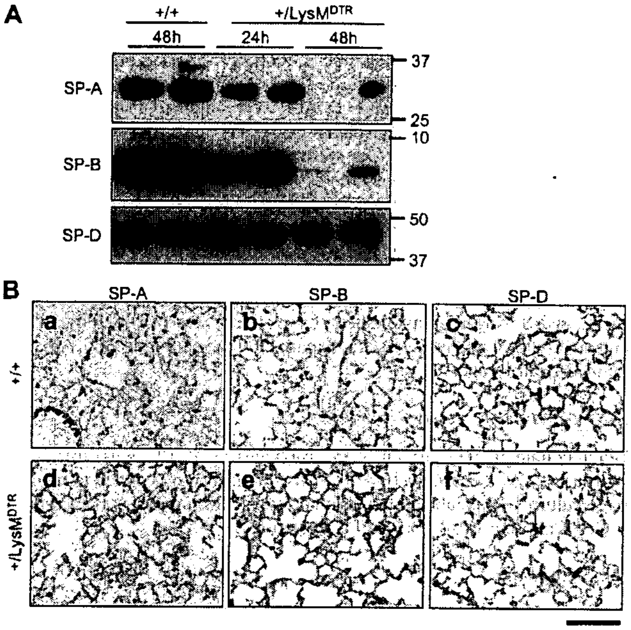

FIGURE 4. Effect of DT administration on surfactant proteins in the lung. *A*, DT at 40 μg/kg was i.p. injected into wild-type mice (+/+) and LysM-DTR (+/LysM^{DTR}) mice. BALF was harvested 24 or 48 h after DT administration and the amount of SPs was analyzed by Western blot analysis using anti-SP-A, anti-SP-B, and anti-SP-D Abs. These results are representative of three independent experiments. *B*, Lungs were obtained from wild-type (+/+) mice (*a–c*) or DT-administered LysM-DTR (+/LysM^{DTR}) mice (*d–f*) 48 h after DT administration and embedded in OCT compound. Cryosections were immunostained with anti-SP-A, anti-SP-B, and anti-SP-D Abs. Scale bar, 100 μm.

Bone marrow transplantation

For each chimera, 1–1.5 × 10^7 bone marrow cells from donor mice were transferred i.v. into recipient mice that had received 9 gray from an x-ray irradiation system, the Gammacell 40 Exactor (^{137}Cs; MDS Nordion) before transfer. The recipient mice were analyzed 6–10 wk after reconstitution.

Results

Generation of LysM-DTR mice

To establish the inducible macrophage depletion mice, we generated LysM-DTR mice in which human DTR was expressed under the control of the *LysM* gene, which is specifically expressed in myelomonocytic cells such as macrophages and monocytes (21–23). Human *DTR* cDNA was introduced into the endogenous ATG start site within the first exon of the *LysM* gene (Fig. 1*A*). The linearized targeting construct was transfected into ES cells, and heterozygous ES cells carrying a human DTR knock-in allele were aggregated with blastocysts to generate LysM-DTR chimeric mice. The chimeric mice were then crossed with C57BL/6 wild-type mice to obtain LysM-DTR heterozygous animals. Homologous recombination of LysM-DTR mice was confirmed by Southern blot analysis (Fig. 1*B*).

We first examined the expression levels of human DTR in the cells from LysM-DTR mice. FACS analysis revealed that human DTR was expressed on the peritoneal macrophages from LysM-DTR mice (Fig. 1*C*). In contrast, the DTR expression was not detected on the surface of peritoneal B cells from LysM-DTR mice. Surface expression of human DTR was also detected on thioglycollate-elicited peritoneal macrophages and bone marrow-derived macrophages from LysM-DTR mice (data not shown). We next examined whether the macrophages from LysM-DTR mice were sensitive to DT. When the thioglycollate-elicited macrophages from LysM-DTR mice were treated with DT, the cells were killed in a dose-dependent manner (Fig. 1*D*). In contrast, the macrophages from wild-type mice were completely resistant to DT. Furthermore, when DT was i.p. injected into LysM-DTR mice, peritoneal macrophages (F4/80$^+$) but not B cells (B220$^+$), were selectively killed (Fig. 1*E*). These results indicated that macrophages from knock-in mice expressed the functional human DTR on the cell surface.

DT administration causes severe lung injury in LysM-DTR mice

We next examined the effects of DT injection on LysM-DTR mice. Various amounts of DT were i.p. injected into LysM-DTR mice, and the injection of a high dose of DT killed the mice (Fig. 2*A*). When 40 μg/kg DT was injected into the transgenic mice, all mice showed hypomotility, hunched posture, and ruffled fur and died within 96 h. In the case of 10 μg/kg injection, half of the mice were killed within 1 wk after injection. In contrast, none of the wild-type mice were killed by the administration of 40 μg/kg DT.

Lactose dehydrogenase levels in the serum of LysM-DTR mice were increased by >7-fold following the administration of 40 μg/kg DT, suggesting severe damage in certain tissues (data not shown). Macroscopic observation revealed that the lungs

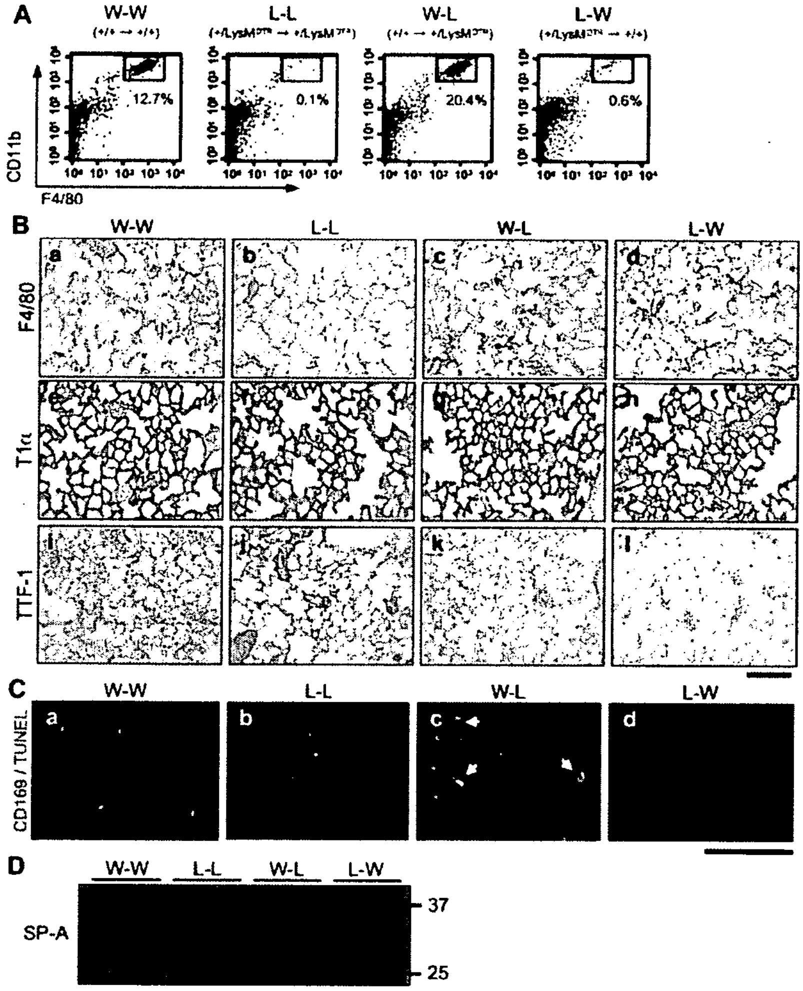

FIGURE 5. Generation of bone marrow chimeric mice. Bone marrow chimeric mice were prepared by lethal irradiation of recipient mice and reconstitution with donor bone marrow cells (donor → recipient; W-W (+/+ → +/+), L-L (+/LysM^{DTR} → +/LysM^{DTR}), W-L (+/+ → +/LysM^{DTR}), L-W (+/LysM^{DTR} → +/+)). Eight to ten weeks after reconstitution, 10 μg/kg DT was i.p. injected into these mice. *A*, Peritoneal cells were harvested 48 h after DT administration and stained with anti-F4/80 and anti-CD11b Abs to detect peritoneal macrophages. *B*, Lungs were obtained from these mice 48 h after DT administration. Sections were immunostained with F4/80 (*a–d*), T1α (*e–h*), and TTF-1 (*i–l*) for alveolar macrophages, AE1 cells, and AE2 cells, respectively. *C*, Sections were double stained with anti-CD169 Ab (red), a marker for alveolar macrophages, and TUNEL (green). Arrows indicate macrophages engulfing apoptotic cells. *D*, BALF was harvested from these mice 48 h after DT administration and SP content was analyzed by Western blot analysis using anti-SP-A Ab. These results are representative of two independent experiments.

had a hemorrhagic appearance (Fig. 2*B*). Histological analysis of the lungs demonstrated that the alveolar walls became thick and the alveolar spaces were diminished (Fig. 2*C*). Moreover, RBC were notably expanded in the interstitial mesenchyme, indicating severe congestion in the lungs. We also microscopically observed other organs, including the heart, kidney, and liver. However, none of these organs showed any abnormalities except the liver that showed slight congestion (data not shown). These results indicated that the lungs were primarily injured in LysM-DTR mice by DT administration.

DT is integrated into cells through its receptor and induces apoptosis by ADP ribosylation of elongation factor 2 (15, 24, 25). We next performed TUNEL staining with the lung sections to detect apoptotic cells. In wild-type mice, no TUNEL-positive cells were observed in the lungs by DT administration (Fig. 2*D*). In contrast, a large number of cells became TUNEL-positive in the lungs of LysM-DTR mice 24 h after DT administration. TUNEL-positive cells were located in the epithelial layer of alveoli as well as inside the alveolar space, indicating that some epithelial cells as well as alveolar macrophages underwent apoptosis by DT. We also performed TUNEL staining with the sections of other tissues. Macrophages in several organs also showed TUNEL-positive staining. However, we could detect neither TUNEL-positive cardiomyocytes nor hepatocytes in the LysM-DTR mouse injected with DT (data not shown).

The alveolar epithelial type II cells are deleted by DT in LysM-DTR mice

The lung alveolar epithelial layer consists of alveolar epithelial type I (AE1) cells and AE2 cells. While AE1 cells cover up to 95% of the surface area of the lungs and are responsible for gas exchange, AE2 cells occupy only 5% of the surface area and produce and secrete the surface-active agents collectively known as surfactants. It has been reported that both alveolar macrophages and AE2 cells express the LysM gene (26, 27). Therefore, in the present study it was most likely that both alveolar macrophages and AE2 cells expressed human DTR and that they were killed by DT administration. To assess this speculation, immunohistochemical analysis for alveolar macrophages and AE2 cells was performed in the lung sections of DT-administered mice. F4/80, T1α, and TTF-1 were used as specific markers of alveolar macrophages, AE1 cells, and AE2 cells, respectively (28–31). The number of both alveolar macrophages and AE2 cells were notably decreased by DT administration to LysM-DTR mice, while that of AE1 cells was not affected (Fig. 3*A*). TTF-1 was also expressed in epithelial cells lining conducting airways (Fig. 3, *Ac* and *Af*, *lower right area* for both wild-type and LysM-DTR mice); however, DT administration had a negligible effect on the epithelial cells lining conducting airways. To further confirm the absence of AE2 cells in LysM-DTR mice injected with DT, the lung sections were analyzed by transmission electron microscopy. In wild-type mice, AE2 cells were located at the alveolar corners and displayed typical cuboidal features with lamellar bodies (Fig.

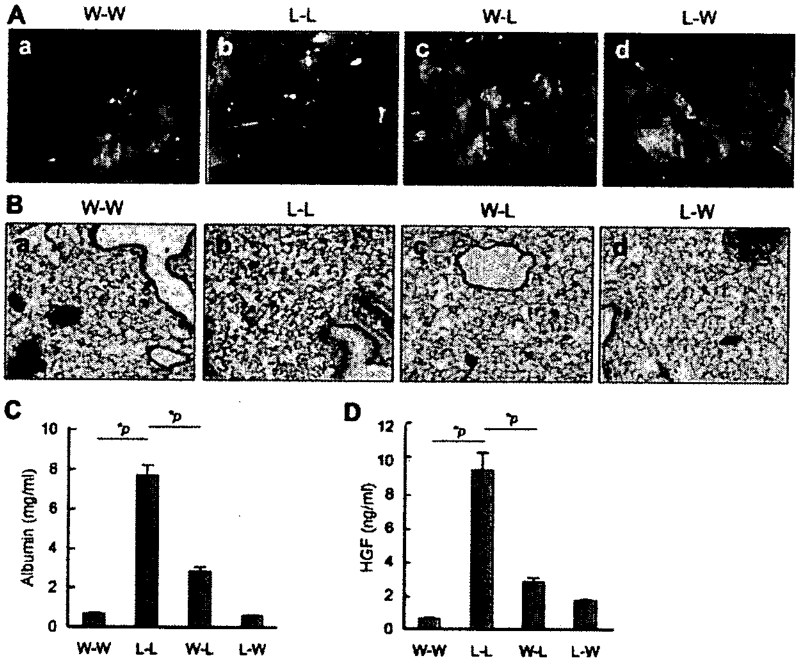

FIGURE 6. Alveolar macrophages decreased pathological changes in the lung injury by DT treatment. DT at 10 μg/kg was i.p. injected into bone marrow chimeric mice (donor → recipient; W-W (+/+ → +/+), L-L (+/LysM^{DTR} → +/LysM^{DTR}), W-L (+/+ → +/LysM^{DTR}), and L-W (+/LysM^{DTR} → +/+)). Mice were sacrificed 24 h after DT administration. *A*, Macroscopic observation of the lung. *B*, Lungs were fixed with 4% paraformaldehyde and embedded in paraffin. Sections were stained with H&E. *C* and *D*, Concentrations of albumin (*C*) and HGF (*D*) in BALF were measured by ELISA. Mean values are shown with SEM. *, $p < 0.01$.

3, *Ba* and *Bc*, arrow). In contrast, intact AE2 cells were hardly observed in LysM-DTR mice treated with DT (Fig. 3*Bb*). Some apoptotic AE2 cells were found at the alveolar corners in these mice (Fig. 3*Bd*). These results indicated that alveolar macrophages and AE2 cells were ablated by DT administration in LysM-DTR mice.

One of the important roles of AE2 cells is the synthesis and secretion of bioactive SPs, which stabilize alveolar spaces by reducing the surface tension of alveoli (32, 33). Thus, it was expected that the ablation of AE2 cells led to the depletion of SPs in alveolar spaces. We next analyzed the effect of DT administration on SPs in BALF. Although the amount of SP-D was not altered, those of SP-A and SP-B were notably decreased by DT administration (Fig. 4*A*). Reduced production of SPs was also confirmed by immunohistochemistry with anti-SP Abs. As shown in Fig. 4*B*, cells producing SP-A, -B, and -D were detected in the lung sections of wild-type mice. In contrast, few SP-producing cells were detected in the lungs of LysM-DTR mice with DT injection. These results indicated that DT administration to LysM-DTR mice induced apoptosis in AE2 cells and caused respiratory failure due to the decreased amount of surfactants.

Contribution of macrophages to lung pathology in the LysM-DTR mice

In LysM-DTR mice, DT administration resulted in the ablation of AE2 cells as well as alveolar macrophages and caused severe respiratory failure possibly due to the decreased amount of SPs. To examine how the ablation of alveolar macrophages contributed to lung pathology in the mice, we performed transplantation of bone marrow cells from wild-type mice into LysM-DTR mice that had been lethally irradiated. Six weeks after the bone marrow transplantation, the sensitivity of peritoneal macrophages to DT was determined in these mice. As shown in Fig. 5*A*, peritoneal macrophages were completely resistant to DT in the LysM-DTR mice reconstituted with wild-type bone marrow cells (W-L mice), whereas these cells were deleted by DT administration in the LysM-DTR mice reconstituted with LysM-DTR bone marrow cells (L-L mice). Consistent with this, alveolar macrophages were not ablated by DT injection in the W-L mice (Fig. 5*Bc*). Some alveolar macrophages in the DT-treated W-L mice phagocytosed apoptotic cells (possibly apoptotic AE2 cells), indicating that DT-resistant, functional alveolar macrophages were successfully reconstituted in the W-L mice. (Fig. 5*Cc*, arrow) In contrast, AE2 cells both in the L-L and the W-L mice were almost completely deleted by DT administration (Fig. 5, *Bj* and *Bk*). We also examined the amount of SP-A in BALF, and found that it was greatly reduced both in the W-L and the L-L mice (Fig. 5*D*). These results indicated that the W-L mice showed selective deletion of AE2 cells with intact alveolar macrophages by DT administration.

We then compared the severity of lung injury induced by DT administration between W-L mice and L-L mice. Although both mice were killed by DT administration, macroscopic observation indicated that lung congestion seemed to be more severe in the L-L mice than in the W-L mice (Fig. 6*A*). Histological examination also gave the same results (Fig. 6*B*). The early phase of lung injury caused by LPS or bleomycin is often associated with an inflammatory reaction, including neutrophil recruitment. However, few neutrophils were observed in the injured lungs even in the presence of alveolar macrophages (W-L mice), indicating that the deletion of AE2 cells by DT administration to LysM-DTR mice did not induce any inflammatory reactions.

To further evaluate the severity of lung injury, we examined the leakage of albumin into alveolar spaces upon DT administration. As shown in Fig. 6*C*, albumin concentrations were much higher in BALF from L-L mice than in that from the W-L mice. No leakage of albumin was observed in WT mice reconstituted with LysM-DTR bone marrow cells (L-W mice) in which alveolar macrophages but not AE2 cells were deleted by DT. These results indicate that the injury of AE2 cells is a major contributor to respiratory failure in DT-treated LysM-DTR mice and that the presence of macrophages diminishes this noninflammatory lung injury caused by AE2 cell deletion.

Production of cytokines in DT-treated LysM-DTR mice

We next examined the concentrations of several cytokines in BALF from these mice. We could not detect the production of either inflammatory cytokines such as TNF-α, or immunoregulatory cytokines such as IL-10 and TGF-β in BALF from any of these mice (data not shown). This is consistent with the histological findings of no inflammatory cells in the lungs of DT-treated mice (W-L and L-L). The HGF is considered to be a candidate growth factor for AE2 cells and is produced by bronchial epithelial cells as well as alveolar macrophages engulfing dying neutrophils in a mouse model of bacterial pneumonia (34). Therefore, we measured HGF concentrations in BALF from these mice. As shown in Fig. *6D*, BALF from DT-treated L-L mice contained a larger amount of HGF than those from W-L mice. This result suggests that the amount of HGF is correlated with the severity of the lung injury caused by AE2 cell deletion and that alveolar macrophages do not contribute to HGF production in noninflammatory AE2 cell injury.

Discussion

To explore the pathophysiology of respiratory distress, several animal models have been used as acute lung injury models. The intratracheal instillation of bleomycin in rodents has been widely used as a model to study the mechanisms of lung injury and repair. In this model, the administration of bleomycin induces early inflammatory responses followed by fibrosis. Histological examination demonstrated that both vascular endothelial cells and AE1 cells, but not AE2 cells, were specifically injured in the lungs of mice treated with bleomycin (35). However, the pathogenesis of the injury and of the subsequent lung disease caused by bleomycin remains obscure. Intratracheal instillation of LPS also induces a massive infiltration of inflammatory cells, including neutrophils and macrophages, causing acute respiratory distress (36, 37). This model, at least in part, represents infection-induced acute respiratory distress syndrome (ARDS) in human. However, the precise mechanism of LPS-induced lung injury remains elusive.

In this study we established transgenic mice expressing human DTR in AE2 cells as well as macrophages. When DT was injected into the transgenic mice AE2 cells selectively underwent apoptosis and the mice showed lethal respiratory failure, possibly due to a rapid decrease in the amount of surfactants produced by AE2 cells. DT injection also killed alveolar macrophages in theses mice. Bone marrow transplantation from wild-type mice could not rescue the lethal phenotype of the LysM-DTR mice, indicating that the ablation of AE2 cells is primarily responsible for the respiratory failure in the mice injected with DT. To our knowledge, this transgenic mouse line is the only mouse model of acute respiratory distress that is possibly due to the selective injury of AE2 cells and the subsequently reduced production of surfactants. In addition to the unique mechanism of acute lung injury in these mice, lung injury was easily and reproducibly induced by i.p. injection of DT, whereas intratracheal instillation of the reagent is required for bleomycin- or LPS-induced acute lung injury in mice.

Injury or apoptosis of AE2 cells has been reported to play an important role in the pathogenesis of several lung diseases. Hypoxia, an important feature of acute lung injury, has been shown to induce apoptosis in AE2 cells in vitro (38). Chronic hypoxia has also been shown to cause morphological changes of AE2 cells including delamellation in vivo (39), suggesting the functional failure of AE2 cells in hypoxia-induced lung injury or fibrosis. In other studies AE2 cells have been reported to express the Fas receptor, a transmembrane protein that transduces death signals upon stimulation (40, 41). When primary cultured AE2 cells were treated with the Fas ligand (FasL) the cells underwent apoptosis in vitro. Moreover, intratracheal administration of FasL or agonistic anti-Fas Ab induces AE2 cell death in vivo (40–42). A considerable amount of the soluble FasL, produced by shedding of the membrane-bound form (43, 44), was detected in BALF of ARDS patients (45), suggesting that AE2 cells could be damaged by FasL/Fas activation in ARDS. As a matter of fact, abnormal surfactant function and changes in the surfactant subfraction, including a decrease in the amount of SPs, were observed in ARDS patients (33, 46–49). Taking these observations into consideration, it is possible that in some ARDS cases AE2 cell death is at least partly responsible for the pathogenesis of ARDS. In this respect the pathology of respiratory failure in the LysM-DTR mouse partly resembles that in human ARDS and, thus, this system will provide a new animal model to investigate the pathophysiology of human ARDS.

In this study we found that the presence of macrophages diminished lung injury caused by AE2 cell deletion. Although it is likely that alveolar macrophages contribute to the protective effects, we cannot deny the possibility that lung interstitial macrophages or macrophages in other organs, such as Kupffer cells, may also contribute to some extent to diminishing lung damage in this model of noninflammatory lung injury. In the acute phase of tissue injury macrophages often perform injury-inducing roles. For instance, the depletion of macrophages in the early phase of carbon tetrachloride-induced liver injury resulted in reduced scarring and fewer myofibroblasts (50). In acute rejection of renal transplantation, infiltrating macrophages promoted tissue damage (51). In this study, by contrast, alveolar macrophages contributed to the reduction of lung injury and serum albumin leakage into alveolar spaces caused by AE2 cell depletion. This result suggests that macrophages play protective roles in noninflammatory tissue injury. In the DT-treated W-L mice, alveolar macrophages phagocytosed apoptotic AE2 cells. This clearance of dying cells by macrophages may be involved in the protective effects. During the late course of inflammation, prompt elimination of neutrophils by macrophages is required for the resolution of inflammation and normal tissue repair (7, 8). The hyaluronan receptor CD44 plays an important role in the phagocytosis of apoptotic neutrophils by macrophages. CD44-deficient mice have been shown to succumb to unremitting inflammation in association with impaired clearance of apoptotic neutrophils in bleomycin-induced acute lung injury (52, 53). Although the lung injury caused by AE2 cell depletion is not associated with the infiltration of neutrophils, the clearance of dying parenchymal cells by macrophages may be a critical factor determining the degree of tissue damages in such noninflammatory tissue injury.

HGF is considered to play an important role in the repair of the pulmonary epithelium in acute lung injury. In mouse bacterial pneumonia the expression of HGF in the lung showed a biphasic pattern (34); that is, bronchial epithelial cells produced the cytokine in the early phase of infection and alveolar macrophages engulfing dying neutrophils produced it in the late phase of infection. In the present study, HGF was produced in acute lung injury caused by the deletion of AE2 cells, and the expression levels in L-L mice were higher than those in W-L mice. These results suggest that bronchial epithelial cells, but not alveolar macrophages, are the major producers of HGF in the case of noninflammatory lung injury without any infiltration of neutrophils. The precise mechanisms of HGF production by bronchial epithelial cells are not known. Because the presence of alveolar macrophages that phagocytosed dying AE2 cells reduced the levels of HGF in lung injury in this study, cellular components released from dying AE2 cells may stimulate HGF production by bronchial epithelial cells.

LysM-DTR mice are also expected to serve as a useful model to study the regeneration of AE2 cells. AE2 cells are considered to be stem cells of the adult alveolar epithelium (54). Primary cultured AE2 cells differentiate into AE1 cells under certain conditions in vitro (55, 56). After lung injury, AE2 cells divide and differentiate into AE1 cells in vivo (57, 58). In the present study most AE2 cells were killed in LysM-DTR mice by DT administration. We could not monitor the course of repair for AE2 cell injury by i.p. DT administration because of early death. However, if AE2 cells in a regional region of lung alveoli are ablated by intratracheal instillation of DT, it may be possible to observe the course of lung repair after AE2 cells are selectively injured.

Acknowledgments

We thank Dr. M. Scharff and Dr. B. Diamond for NSO^{Bcl-2} cell, Dr. S. Nagata for pEF-BOS-EX vector and anti-F4/80 Ab (6-16A), and H. Matsuda for secretarial assistance. Anti-T1α Ab (clone 8.1.1) developed by Dr. Farr was obtained from the Developmental Studies Hybridoma Bank developed under the auspices of the National Institute of Child Health and Human Development and maintained by Department of Biological Sciences, University of Iowa, (Iowa City, IA).

Disclosures

Y. Miyake and M. Tanaka, together with RIKEN, have a pending patent on the LysM-DTR mouse as a mouse model for acute respiratory distress syndrome.

References

1. Duffield, J. S. 2003. The inflammatory macrophage: a story of Jekyll and Hyde. *Clin. Sci.* 104: 27–38.
2. Goerdt, S., and C. E. Orfanos. 1999. Other functions, other genes: alternative activation of antigen-presenting cells. *Immunity* 10: 137–142.
3. Gordon, S. 2003. Alternative activation of macrophages. *Nat. Rev. Immunol.* 3: 23–35.
4. Henson, P. M., D. L. Bratton, and V. A. Fadok. 2001. Apoptotic cell removal. *Curr. Biol.* 11: R795–R805.
5. Lauber, K., S. G. Blumenthal, M. Waibel, and S. Wesselborg. 2004. Clearance of apoptotic cells: getting rid of the corpses. *Mol. Cell* 14: 277–287.
6. Savill, J., and V. Fadok. 2000. Corpse clearance defines the meaning of cell death. *Nature* 407: 784–788.
7. Haslett, C. 1999. Granulocyte apoptosis and its role in the resolution and control of lung inflammation. *Am. J. Respir. Crit. Care Med.* 160: S5–S11.
8. Lawrence, T., D. A. Willoughby, and D. W. Gilroy. 2002. Anti-inflammatory lipid mediators and insights into the resolution of inflammation. *Nat. Rev. Immunol.* 2: 787–795.
9. Voll, R. E., M. Herrmann, E. A. Roth, C. Stach, J. R. Kalden, and I. Girkontaite. 1997. Immunosuppressive effects of apoptotic cells. *Nature* 390: 350–351.
10. Byrne, A., and D. J. Reen. 2002. Lipopolysaccharide induces rapid production of IL-10 by monocytes in the presence of apoptotic neutrophils. *J. Immunol.* 168: 1968–1977.
11. Asano, K., M. Miwa, K. Miwa, R. Hanayama, H. Nagase, S. Nagata, and M. Tanaka. 2004. Masking of phosphatidylserine inhibits apoptotic cell engulfment and induces autoantibody production in mice. *J. Exp. Med.* 200: 459–467.
12. Saito, M., T. Iwawaki, C. Taya, H. Yonekawa, M. Noda, Y. Inui, E. Mekada, Y. Kimata, A. Tsuru, and K. Kohno. 2001. Diphtheria toxin receptor-mediated conditional and targeted cell ablation in transgenic mice. *Nat. Biotechnol.* 19: 746–750.
13. Pappenheimer, A. M., Jr., A. A. Harper, M. Moynihan, and J. P. Brockes. 1982. Diphtheria toxin and related proteins: effect of route of injection on toxicity and the determination of cytotoxicity for various cultured cells. *J. Infect. Dis.* 145: 94–102.
14. Mitamura, T., S. Higashiyama, N. Taniguchi, M. Klagsbrun, and E. Mekada. 1995. Diphtheria toxin binds to the epidermal growth factor (EGF)-like domain of human heparin-binding EGF-like growth factor/diphtheria toxin receptor and inhibits specifically its mitogenic activity. *J. Biol. Chem.* 270: 1015–1019.
15. Naglich, J. G., J. E. Metherall, D. W. Russell, and L. Eidels. 1992. Expression cloning of a diphtheria toxin receptor: identity with a heparin-binding EGF-like growth factor precursor. *Cell* 69: 1051–1061.
16. Jung, S., D. Unutmaz, P. Wong, G. Sano, K. De los Santos, T. Sparwasser, S. Wu, S. Vuthoori, K. Ko, F. Zavala, et al. 2002. In vivo depletion of $CD11c^+$ dendritic cells abrogates priming of $CD8^+$ T cells by exogenous cell-associated antigens. *Immunity* 17: 211–220.
17. Nagy, A., J. Rossant, R. Nagy, W. Abramow-Newerly, and J. C. Roder. 1993. Derivation of completely cell culture-derived mice from early-passage embryonic stem cells. *Proc. Natl. Acad. Sci. USA* 90: 8424–8428.
18. Laird, P. W., A. Zijderveld, K. Linders, M. A. Rudnicki, R. Jaenisch, and A. Berns. 1991. Simplified mammalian DNA isolation procedure. *Nucleic Acids Res.* 19: 4293.
19. Murai, K., H. Murakami, and S. Nagata. 1998. Myeloid-specific transcriptional activation by murine myeloid zinc-finger protein 2. *Proc. Natl. Acad. Sci. USA* 95: 3461–3466.
20. Ray, S., and B. Diamond. 1994. Generation of a fusion partner to sample the repertoire of splenic B cells destined for apoptosis. *Proc. Natl. Acad. Sci. USA* 91: 5548–5551.
21. Cross, M., I. Mangelsdorf, A. Wedel, and R. Renkawitz. 1988. Mouse lysozyme M gene: isolation, characterization, and expression studies. *Proc. Natl. Acad. Sci. USA* 85: 6232–6236.
22. Cross, M., and R. Renkawitz. 1990. Repetitive sequence involvement in the duplication and divergence of mouse lysozyme genes. *EMBO J.* 9: 1283–1288.
23. Clausen, B. E., C. Burkhardt, W. Reith, R. Renkawitz, and I. Forster. 1999. Conditional gene targeting in macrophages and granulocytes using LysMcre mice. *Transgenic Res.* 8: 265–277.
24. Honjo, T., Y. Nishizuka, and O. Hayaishi. 1968. Diphtheria toxin-dependent adenosine diphosphate ribosylation of aminoacyl transferase II and inhibition of protein synthesis. *J. Biol. Chem.* 243: 3553–3555.
25. Van Ness, B. G., J. B. Howard, and J. W. Bodley. 1980. ADP-ribosylation of elongation factor 2 by diphtheria toxin: isolation and properties of the novel ribosyl-amino acid and its hydrolysis products. *J. Biol. Chem.* 255: 10717–10720.
26. Spicer, S. S., R. Frayser, G. Virella, and B. J. Hall. 1977. Immunocytochemical localization of lysozymes in respiratory and other tissues. *Lab. Invest.* 36: 282–295.
27. Singh, G., S. L. Katyal, W. E. Brown, D. L. Collins, and R. J. Mason. 1988. Pulmonary lysozyme—a secretory protein of type II pneumocytes in the rat. *Am. Rev. Respir. Dis.* 138: 1261–1267.
28. Farr, A., A. Nelson, and S. Hosier. 1992. Characterization of an antigenic determinant preferentially expressed by type I epithelial cells in the murine thymus. *J. Histochem. Cytochem.* 40: 651–664.
29. Holzinger, A., S. Dingle, P. A. Bejarano, M. A. Miller, T. E. Weaver, R. DiLauro, and J. A. Whitsett. 1996. Monoclonal antibody to thyroid transcription factor-1: production, characterization, and usefulness in tumor diagnosis. *Hybridoma* 15: 49–53.
30. Ikeda, K., J. C. Clark, J. R. Shaw-White, M. T. Stahlman, C. J. Boutell, and J. A. Whitsett. 1995. Gene structure and expression of human thyroid transcription factor-1 in respiratory epithelial cells. *J. Biol. Chem.* 270: 8108–8114.
31. Kotton, D. N., B. Y. Ma, W. V. Cardoso, E. A. Sanderson, R. S. Summer, M. C. Williams, and A. Fine. 2001. Bone marrow-derived cells as progenitors of lung alveolar epithelium. *Development* 128: 5181–5188.
32. Fehrenbach, H. 2001. Alveolar epithelial type II cell: defender of the alveolus revisited. *Respir. Res.* 2: 33–46.
33. Lewis, J. F., and R. Veldhuizen. 2003. The role of exogenous surfactant in the treatment of acute lung injury. *Annu. Rev. Physiol.* 65: 613–642.
34. Morimoto, K., H. Amano, F. Sonoda, M. Baba, M. Senba, H. Yoshimine, H. Yamamoto, T. Ii, K. Oishi, and T. Nagatake. 2001. Alveolar macrophages that phagocytose apoptotic neutrophils produce hepatocyte growth factor during bacterial pneumonia in mice. *Am. J. Respir. Cell Mol. Biol.* 24: 608–615.
35. Jules-Elysee, K., and D. A. White. 1990. Bleomycin-induced pulmonary toxicity. *Clin. Chest Med.* 11: 1–20.
36. Reutershan, J., A. Basit, E. V. Galkina, and K. Ley. 2005. Sequential recruitment of neutrophils into lung and bronchoalveolar lavage fluid in LPS-induced acute lung injury. *Am. J. Physiol.* 289: L807–L815.
37. Schnyder-Candrian, S., V. F. Quesniaux, F. Di Padova, I. Maillet, N. Noulin, I. Couillin, R. Moser, F. Erard, B. B. Vargaftig, B. Ryffel, and B. Schnyder. 2005. Dual effects of p38 MAPK on TNF-dependent bronchoconstriction and TNF-independent neutrophil recruitment in lipopolysaccharide-induced acute respiratory distress syndrome. *J. Immunol.* 175: 262–269.
38. Krick, S., B. G. Eul, J. Hanze, R. Savai, F. Grimminger, W. Seeger, and F. Rose. 2005. Role of hypoxia-inducible factor-1α in hypoxia-induced apoptosis of primary alveolar epithelial type II cells. *Am. J. Respir. Cell Mol. Biol.* 32: 395–403.
39. Sulkowska, M. 1997. Morphological studies of the lungs in chronic hypobaric hypoxia. *Pol. J. Pathol.* 48: 225–234.
40. Matute-Bello, G., W. C. Liles, C. W. Frevert, M. Nakamura, K. Ballman, C. Vathanaprida, P. A. Kiener, and T. R. Martin. 2001. Recombinant human Fas ligand induces alveolar epithelial cell apoptosis and lung injury in rabbits. *Am. J. Physiol.* 281: L328–L335.
41. Fine, A., N. L. Anderson, T. L. Rothstein, M. C. Williams, and B. R. Gochuico. 1997. Fas expression in pulmonary alveolar type II cells. *Am. J. Physiol.* 273: L64–L71.
42. Matute-Bello, G., R. K. Winn, M. Jonas, E. Y. Chi, T. R. Martin, and W. C. Liles. 2001. Fas (CD95) induces alveolar epithelial cell apoptosis in vivo: implications for acute pulmonary inflammation. *Am. J. Pathol.* 158: 153–161.
43. Tanaka, M., T. Suda, T. Takahashi, and S. Nagata. 1995. Expression of the functional soluble form of human fas ligand in activated lymphocytes. *EMBO J.* 14: 1129–1135.
44. Tanaka, M., T. Itai, M. Adachi, and S. Nagata. 1998. Downregulation of Fas ligand by shedding. *Nat. Med.* 4: 31–36.
45. Matute-Bello, G., W. C. Liles, K. P. Steinberg, P. A. Kiener, S. Mongovin, E. Y. Chi, M. Jonas, and T. R. Martin. 1999. Soluble Fas ligand induces epithelial cell apoptosis in humans with acute lung injury (ARDS). *J. Immunol.* 163: 2217–2225.
46. Gregory, T. J., W. J. Longmore, M. A. Moxley, J. A. Whitsett, C. R. Reed, A. A. Fowler, 3rd, L. D. Hudson, R. J. Maunder, C. Crim, and T. M. Hyers. 1991. Surfactant chemical composition and biophysical activity in acute respiratory distress syndrome. *J. Clin. Invest.* 88: 1976–1981.

47. Lewis, J. F., and A. H. Jobe. 1993. Surfactant and the adult respiratory distress syndrome. *Am. Rev. Respir. Dis.* 147: 218–233.
48. Veldhuizen, R. A., L. A. McCaig, T. Akino, and J. F. Lewis. 1995. Pulmonary surfactant subfractions in patients with the acute respiratory distress syndrome. *Am. J. Respir. Crit. Care Med.* 152: 1867–1871.
49. Spragg, R. G., and J. F. Lewis. 2003. Surfactant therapy in the acute respiratory distress syndrome. In *Acute Respiratory Distress Syndrome*. M. A. Matthay, ed. Marcel Dekker, New York, pp. 533–562.
50. Duffield, J. S., S. J. Forbes, C. M. Constandinou, S. Clay, M. Partolina, S. Vuthoori, S. Wu, R. Lang, and J. P. Iredale. 2005. Selective depletion of macrophages reveals distinct, opposing roles during liver injury and repair. *J. Clin. Invest.* 115: 56–65.
51. Jose, M. D., Y. Ikezumi, N. van Rooijen, R. C. Atkins, and S. J. Chadban. 2003. Macrophages act as effectors of tissue damage in acute renal allograft rejection. *Transplantation* 76: 1015–1022.
52. Hart, S. P., G. J. Dougherty, C. Haslett, and I. Dransfield. 1997. CD44 regulates phagocytosis of apoptotic neutrophil granulocytes, but not apoptotic lymphocytes, by human macrophages. *J. Immunol.* 159: 919–925.
53. Teder, P., R. W. Vandivier, D. Jiang, J. Liang, L. Cohn, E. Pure, P. M. Henson, and P. W. Noble. 2002. Resolution of lung inflammation by CD44. *Science* 296: 155–158.
54. Uhal, B. D. 1997. Cell cycle kinetics in the alveolar epithelium. *Am. J. Physiol.* 272: L1031–L1045.
55. Danto, S. I., J. M. Shannon, Z. Borok, S. M. Zabski, and E. D. Crandall. 1995. Reversible transdifferentiation of alveolar epithelial cells. *Am. J. Respir. Cell Mol. Biol.* 12: 497–502.
56. Shannon, J. M., S. D. Jennings, and L. D. Nielsen. 1992. Modulation of alveolar type II cell differentiated function in vitro. *Am. J. Physiol.* 262: L427–L436.
57. Evans, M. J., L. J. Cabral, R. J. Stephens, and G. Freeman. 1973. Renewal of alveolar epithelium in the rat following exposure to NO_2. *Am. J. Pathol.* 70: 175–198.
58. Kapanci, Y., E. R. Weibel, H. P. Kaplan, and F. R. Robinson. 1969. Pathogenesis and reversibility of the pulmonary lesions of oxygen toxicity in monkeys, II: ultrastructural and morphometric studies. *Lab. Invest.* 20: 101–118.

Chromosome Research (2007) 15:299–314
DOI: 10.1007/s10577-007-1126-1

© Springer 2007

The Polycomb Group Protein SUZ12 regulates histone H3 lysine 9 methylation and HP1α distribution

Cecile C. de la Cruz[1], Antonis Kirmizis[2], Matthew D. Simon[3], Kyo-ichi Isono[4], Haruhiko Koseki[4] & Barbara Panning[1,5]*
[1]*Department of Biochemistry and Biophysics, University of California San Francisco, San Francisco, CA 94143, USA;* [2]*Wellcome Trust/Cancer Research UK Gurdon Institute, University of Cambridge, Cambridge, CB2 1QN, UK;* [3]*Department of Chemistry, University of California, Berkeley, CA 94720, USA;* [4]*RIKEN Research Center for Allergy and Immunology, 1-7-22 Suehiro, Tsurumi-ku, Yokohama 230-0045, Japan;* [5]*Genentech Hall, Room S372B, 600 16th Street, San Francisco, CA 94143-2200 (94158 for courier delivery), USA; Tel: +1-415-5140745; Fax: +1-415-5144080; E-mail: bpanning@biochem.ucsf.edu*
* *Correspondence*

Received 4 October 2006. Received in revised form and accepted for publication by Nobuo Takagi 10 January 2007

Key words: heterochromatin, histone methylation, polycomb protein

Abstract

Regulation of histone methylation is critical for proper gene expression and chromosome function. Suppressor of Zeste 12 (SUZ12) is a requisite member of the EED/EZH2 histone methyltransferase complexes, and is required for full activity of these complexes *in vitro*. In mammals and flies, SUZ12/Su(z)12 is necessary for trimethylation of histone H3 on lysine 27 (H3K27me3) on facultative heterochromatin. However, Su(z)12 is unique among Polycomb Group Proteins in that *Su(z)12* mutant flies exhibit gross defects in position effect variegation, suggesting a role for Su(z)12 in constitutive heterochromatin formation. We investigated the role of Suz12 in constitutive heterochromatin and discovered that Suz12 is required for histone H3 lysine 9 trimethylation (H3K9me3) in differentiated but not undifferentiated mouse embryonic stem cells. Knockdown of SUZ12 in human cells caused a reduction in H3K27me3 and H3K9me3, and altered the distribution of HP1α. In contrast, EZH2 knockdown caused loss of H3K27me3 but not H3K9me3, indicating that SUZ12 regulates H3-K9 methylation in an EZH2-independent fashion. This work uncovers a role for SUZ12 in H3-K9 methylation.

Introduction

Heterochromatin is the portion of the genome that is cytologically highly condensed. Different sequences are packaged into facultative heterochromatin in each cell type, allowing cells to stably maintain their unique expression patterns. In contrast, constitutive heterochromatin is formed at pericentric and telomeric regions to epigenetically regulate centromere and telomere function in all cell types and developmental stages. Perturbation of heterochromatin can lead to aberrant gene expression and defective chromosome segregation, contributing to cancer and developmental disorders.

In *Drosophila* the Polycomb Group (PcG) protein Suppressor of Zeste 12 (Su(z)12) is implicated in the formation of facultative and constitutive heterochromatin. PcG proteins assemble into several functionally and biochemically distinct complexes, termed Polycomb repressive complexes (PRC), to mediate transcriptional silencing (Lehnertz *et al.* 2003). PRC2-mediated silencing at *Drosophila Hox* loci requires methylation of histone H3 at lysine 27 (H3-K27) and/or lysine 9 (H3-K9) by the Enhancer of

Zeste (E(z)) histone methyltransferase (HMTase) (Breiling *et al.* 2004, Czermin *et al.* 2002, Muller *et al.* 2002). Suppressor of Zeste 12 (Su(z)12) is an essential component of the E(z) HMTase complex (Ketel *et al.* 2005, Nekrasov *et al.* 2005).

Genetic and biochemical analyses in *Drosophila* and *Schizosaccharomyces pombe* also implicate HMTases in the formation of constitutive heterochromatin. Suppressor of variegation 3-9 (Su(var)3-9) is an HMTase that methylates H3-K9 on constitutive heterochromatin (Rea *et al.* 2000). Methylation of H3-K9 generates a binding site for the chromodomain of heterochromatin protein 1 (HP1) (Bannister *et al.* 2001, Lachner *et al.* 2001, Nakayama *et al.* 2001). In addition, Su(var)3-9 and HP1 directly interact (Aagaard *et al.* 1999, Grewal & Moazed 2003, Melcher *et al.* 2000, Yamamoto & Sonoda 2003). It is postulated that propagation of constitutive heterochromatin occurs via a self-sustaining loop in which methylated H3-K9 binds HP1; HP1 in turn recruits more of the methyltransferase (Grewal & Moazed 2003). *Drosophila* mutations in either *Su(var)3-9* or *Su(var)2-5*, the gene encoding HP1, exhibit defects in position effect variegation (PEV), the variable spread of silencing into euchromatic genes ectopically positioned in proximity to constitutive heterochromatin (Reuter & Wolff 1981, Sinclair *et al.* 1989). Su(z)12 is unique among PcG proteins because mutations of Suz12 exhibit strong defects in PEV, implicating this protein in regulation of constitutive heterochromatin (Birve *et al.* 2001).

Mammals assemble constitutive and facultative heterochromatin structures by mechanisms that are homologous to those of *Drosophila*. The mouse homologues of *Su(var)3-9*, *Suvar39h1* and *Suvar39h2*, are required for the accumulation of tri-methylation of lysine 9 on histone H3 (H3K9me3) and of the mammalian HP1 homologues, HP1α, HP1β and HP1γ, on pericentric heterochromatin (Bannister *et al.* 2001, Lachner *et al.* 2001, Nakayama *et al.* 2001, Rice *et al.* 2003). An HMTase complex that contains a murine homologue of E(z) is required for enrichment of H3K27me3 on the facultative heterochromatin of the inactive X chromosome (Erhardt *et al.* 2003, Plath *et al.* 2003, Silva *et al.* 2003). Human EZH2, in complex with different isoforms of another PcG protein EED, exhibits HMTase activity towards H3-K27, histone H1 lysine 26, and limited activity for H3-K9 *in vitro* (Cao *et al.* 2002, Kuzmichev *et al.* 2002, 2004). SUZ12, the human homologue of the fly PcG protein Suz(12), is a component of EED/EZH2 complexes and is necessary for the H3K27me3 HMTase activity of the EED/EZH2 complex *in vivo* (Cao & Zhang 2004b, Kirmizis *et al.* 2004, Pasini *et al.* 2004).

In addition to interacting with EZH2 and EED, SUZ12 also binds to HP1α (Cao & Zhang 2004a, Yamamoto *et al.* 2004), suggesting that, like the fly homologue, SUZ12 may play a role in constitutive heterochromatin formation in mammalian cells. Levels of murine Suz12 remain constant during mouse embryonic stem (ES) cell differentiation, while Eed and Ezh2 levels decrease, providing a second line of evidence that Suz12 may function outside the Eed/Ezh2 complexes (de la Cruz *et al.* 2005). To determine whether SUZ12 plays a role in constitutive heterochromatin formation, we examined levels and distribution of H3K9me3 in Suz12 knockout ES cells and discovered that Suz12 is required in a differentiation-dependent manner for proper H3-K9 tri-methylation. Further, we analyzed H3K9me3 and HPα in somatic cells that were depleted of SUZ12 by small interfering RNA (siRNA). Knockdown of SUZ12 resulted in a significant decrease of H3K9me3 and in a redistribution of HP1α. SUZ12 knockdown also produced nuclear defects consistent with abnormalities in chromosome segregation, implicating SUZ12 in the regulation of pericentric heterochromatin formation and centromere function. In contrast, siRNA-mediated knockdown of EZH2, which reduced levels of H3K27me3, did not alter the abundance or localization of H3K9me3. These results suggest a role of SUZ12 in H3-K9 methylation, that occurs in a manner independent of its interaction with EZH2.

Materials and methods

Antibodies

The chicken H3K9me3 antibody has been previously described (Plath *et al.* 2003). Experiments using H3K27me3 antibodies employed either a previously characterized chicken H3K27me3 antibody (Plath *et al.* 2003) or a mouse monoclonal antibody (ab6002, Abcam Inc.). Mouse monoclonal HP1α antibody (MAB3584) purchased from Chemicon was used for immunofluorescence and the mouse monoclonal

HP1α antibody (07-346) purchased from Upstate was used for Western blots. SUV39H1 antibody was obtained from Upstate (05615). Rabbit EZH2 and SUZ12 antibodies have been described previously (Cao *et al.* 2002, Kirmizis *et al.* 2004). The anti-histone H3 antibody (ab1791, Abcam Inc.), anti-actin antibody (sc-1615, Santa Cruz Biotechnology) and anti-gamma tubulin antibody (GTU88, Sigma) was used for Western blots. The H3K9me3 antibody (ab8898, Abcam Inc.) and a polyclonal rabbit anti-Myc antibody (ab9106, Abcam Inc.) were used for Western blotting

Cell culture

The IMR90 human female fibroblasts, WI38 human female fibroblasts, and HEL299 human male fibroblasts were purchased from American Type Culture Collection (ATCC) and cultured according to ATCC's handling procedures. HEK 293 cells were cultured in Dulbecco's modified Eagle's media with 10% fetal bovine serum and antibiotics. Suz12 null ES cells were described in Lee *et al.* 2006. ES cells were cultured using standard conditions and differentiation of ES cells was carried out as described in Plath *et al.* 2003.

siRNA transfection

SUZ12 siRNA SMARTpool (M0069570050), EZH2 siRNA SMARTpool (M00421800) and control GFP siRNA oligonucleotides (D0013000120) were obtained from Dharmacon Research Inc. siRNA duplexes were transfected into IMR90 cells using Lipofectamine 2000 (Invitrogen) according to the manufacturer's instructions. Transfected cells were incubated with the siRNA for 72 h, at which time they were harvested and re-plated at the original starting density. Cells were then re-transfected 6 h after replating with the oligonucleotides and incubated for an additional 66 h. After 6 days post-initial siRNA transfection the cells were harvested and processed for immunofluorescence and Western blot analysis as detailed below.

Plasmid constructs and transient transfection

The pCMV-Myc-SUZ12 plasmid was a generous gift from Ken Yamamoto. The plasmid was transfected into HEK 293 cells (5×10^6/10-cm plate) using FuGENE6 (Roche Applied Science) according to the manufacturer's conditions.

Immunofluorescence (IF)

All cells were grown on coverslips, with the exception of undifferentiated embryonic stem cells, which were cytospun onto slides for IF. For Triton X-100 cytoskeleton extraction and IF of cells refer to Plath *et al.* 2003. The following secondary and tertiary antibodies were used for IF at a dilution of 1:200 (Vector Labs): Texas Red anti-mouse IgG, Texas Red anti-rabbit IgG, Fluorescein anti-mouse IgG. Cells that were not subjected to Triton X-100 extraction were fixed with 4% paraformaldehyde for 10 min, then directly incubated in blocking buffer as described in (Plath *et al.* 2003).

Western blotting

IMR90 cells were harvested from the RNAi experiments and 5×10^5 cells from each treatment were boiled in 20 μl of loading dye (9% 2-mercaptoethanol, 9% SDS, 0.1% bromophenol blue, 30% glycerol) for 10 min. The denatured proteins were separated by SDS/PAGE on a 13% gel and transferred onto a nitrocellulose membrane. The membrane was incubated in blocking buffer (Tris-buffered saline with 0.1% Tween [TBS-T] and 5% nonfat dry milk) overnight at 4°C. The next day the membrane was incubated for 1 h at room temperature with anti-SUZ12 antibody (Kirmizis *et al.* 2004) anti-trimethyl H3-K27 antibody (ab6002, Abcam Inc.), anti-trimethyl H3-K9 antibody (ab8898, Abcam Inc.), anti-histone H3 antibody (ab1791, Abcam Inc.), or anti-actin antibody (sc-1615, Santa Cruz Biotechnology). After washing in TBS-T for 15 min, the blot was incubated for 1 h with a horseradish peroxidase (HRP)-conjugated anti-rabbit secondary antibody (sc-2004, Santa Cruz Biotechnology) or an HRP-conjugated anti-mouse secondary antibody (sc-2005, Santa Cruz Biotechnology) and the signals were visualized by the enhanced chemiluminescence system as described by the manufacturer (RPN2106V, Amersham Biosciences). The H3K9me3 and H3K27me3 signals were quantified using ImageQuant and were normalized to the intensities of the histone H3 bands. Fold changes were calculated from the SUZ12- or EZH2 siRNA-treated samples compared to the mock transfected and GFP siRNA transfected samples.

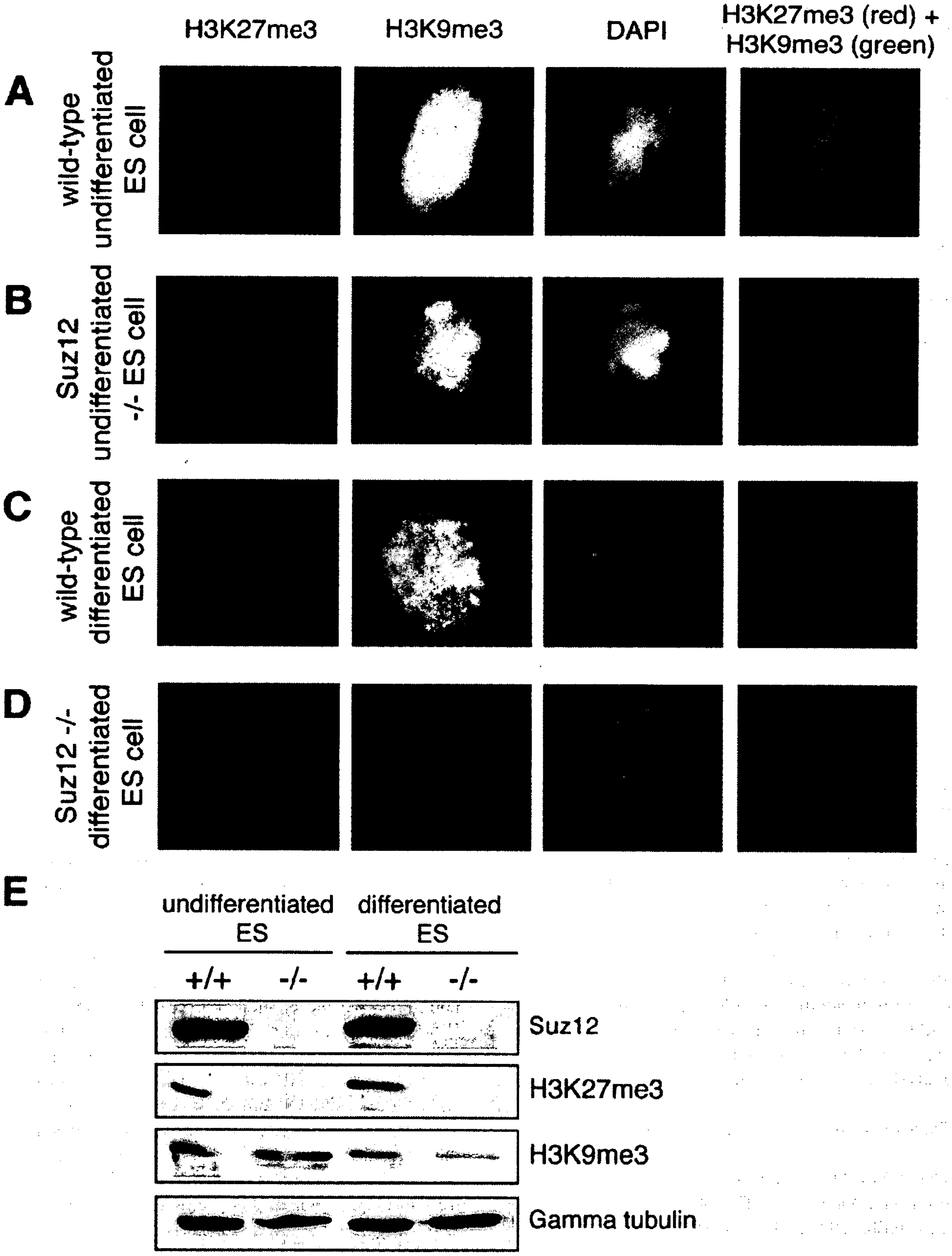
H3K27me3
H3K9me3
DAPI
H3K27me3 (red) + H3K9me3 (green)
A
wild-type undifferentiated ES cell
B
Suz12 undifferentiated -/- ES cell
C
wild-type differentiated ES cell
D
Suz12 -/- differentiated ES cell
E
undifferentiated ES
differentiated ES
+/+
-/-
+/+
-/-
Suz12
H3K27me3
H3K9me3
Gamma tubulin

MBP in vitro binding assays

Human cDNA of SUV39H1 was cloned into the bacterial expression construct pMAL-c2X (NEB). Purification of MBP fusion proteins was performed as outlined by the manufacturer's instructions using amylose resin (NEB). The pull-down binding reaction was performed exactly as described (Tonozuka *et al.* 2004), with the following alterations: 25 μg of MBP-SUV39H1 or MBP was incubated with 1.5 mg cellular extract for 2 h at 4°C. Two washes were performed at 4°C, followed by five washes at room temperature using Ultrafree-MC filters (Millipore).

Image acquisition

Images were acquired using an Olympus BX60 microscope with an Olympus 100× UplanApo oil immersion lens with a numerical aperture of 1.35. A Hamamatsu ORCA-ER camera was used to capture the images, using Openlab 3.1.7 software. Images were globally adjusted for brightness and contrast, merged and pseudo-colored using Adobe Photoshop 7.

Results

Suz12 is required for histone H3-K9 tri-methylation in differentiated cells

To determine whether Suz12 affects constitutive heterochromatin structure in mammalian cells, as has been reported for its fly homolog (Birve *et al.* 2001), we tested if Suz12 regulated the levels and/or distribution of H3K9me3, which is enriched on pericentric heterochromatin (Lachner *et al.* 2001, Peters *et al.* 2001, 2003, Rice *et al.* 2003). We performed co-immunostaining for H3K27me3 and H3K9me3 on wild-type murine ES cells and ES cells lacking *Suz12* (*Suz12* −/−). Wild-type ES cells exhibited a diffusely nuclear pattern of H3K27me3 staining (Figure 1A). Localization of H3K9me3 in wild-type cells was also diffusely nuclear with enrichment on areas of pericentric heterochromatin, as marked by intense DAPI staining (Figure 1A). *Suz12* −/− ES cells lacked detectable amounts of H3K27me3, as previously reported (Fujimura *et al.* 2006), but showed levels and distribution of H3K9me3 similar to wild-type ES cells (Figure 1B). This result indicates that Suz12 is not required for proper H3K9 tri-methylation in undifferentiated ES cells.

Suz12 levels remain high during mouse ES cell differentiation, while Eed and Ezh2 levels decrease dramatically, suggesting that Suz12 may have an Eed/Ezh2-independent function in differentiated cells (de la Cruz *et al.* 2005). To examine whether Suz12 played a role in constitutive heterochromatin in differentiated ES cells, we compared amounts and distribution of H3K9me3 and H3K27me3 in differentiated wild-type and *Suz12* −/− ES cells. Wild-type ES cells contained diffuse nuclear staining of H3K27me3, and clear enrichment of H3K9me3 in areas of constitutive heterochromatin (Figure 1C). In contrast, H3K27me3 was undetectable in differentiated *Suz12* −/− ES cells and overall levels of H3K9me3 were reduced (Figure 1D). Differentiated *Suz12* −/− ES cells still exhibited an enrichment of H3K9me3 at constitutive heterochromatin, but at levels lower than wild-type differentiated ES cells (Figure 1D). Western blotting confirmed that there was a decrease in amounts of H3K9me3 in differentiated but not undifferentiated *Suz12* −/− ES cells (Figure 1E). These data indicate that Suz12 is required for normal levels of H3-K9 tri-methylation in differentiated cells, but not in ES cells.

To further investigate the role of SUZ12 in regulating levels of H3K9me3 in differentiated cells we performed a series of SUZ12 siRNA-mediated knockdown experiments in a primary female human fibroblast cell line (IMR90). Immunostaining of IMR90 cells treated with GFP siRNA showed that SUZ12 levels remained abundant and were identical to non-treated cells, indicating that siRNA treatment did not adversely affect the cells (Figure 2A and C, data not shown). H3K9me3 distribution in these cells was diffusely nuclear, with foci of strong enrichment as well as many speckles. siRNA-mediated knockdown of SUZ12 resulted in loss of SUZ12 in about

Figure 1. Distribution of H3K27me3 and H3K9me3 in wild-type and *Suz12* −/− ES cells. A–D: Immunolocalization of H3K27me3 (first column) and H3K9me3 (second column) in wild-type ES cells (A), *Suz12* −/− ES cells (B), wild-type differentiated ES cells (C), and *Suz12* −/− ES cells (D). Nuclei are stained with DAPI (third column) to visualize nuclei. The merged image (fourth column) consists of H3K27me3 (green) and H3K9me3 (red). E: Western analysis of Suz12, H3K27me3, H3K9me3, and gamma tubulin in undifferentiated wild-type ES cells, undifferentiated *Suz12* −/− ES cells, differentiated wild-type ES cells, and differentiated *Suz12* −/− ES cells.

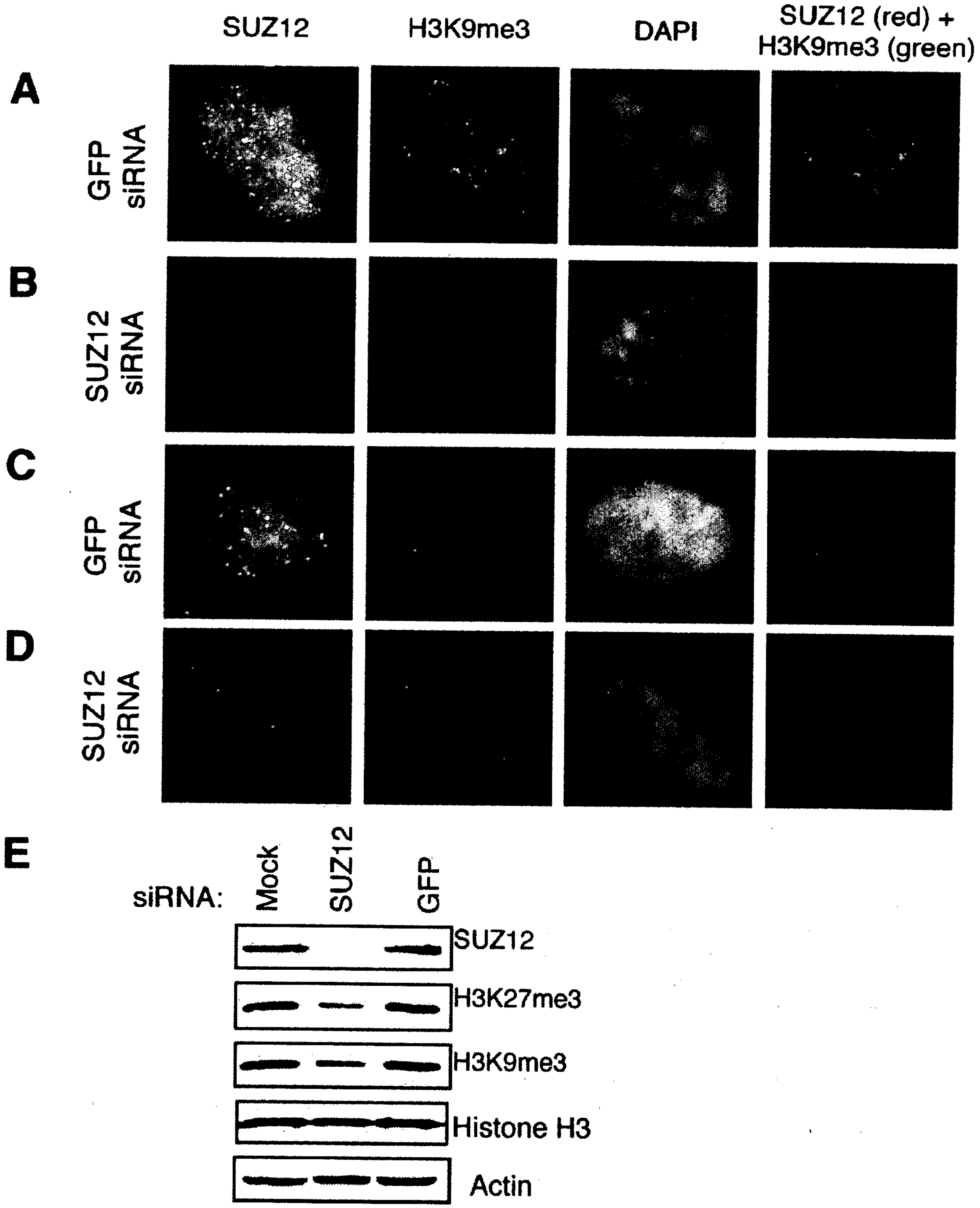
SUZ12
H3K9me3
DAPI
SUZ12 (red) +
H3K9me3 (green)
A
GFP siRNA
B
SUZ12 siRNA
C
GFP siRNA
D
SUZ12 siRNA
E
siRNA:
Mock
SUZ12
GFP
SUZ12
H3K27me3
H3K9me3
Histone H3
Actin

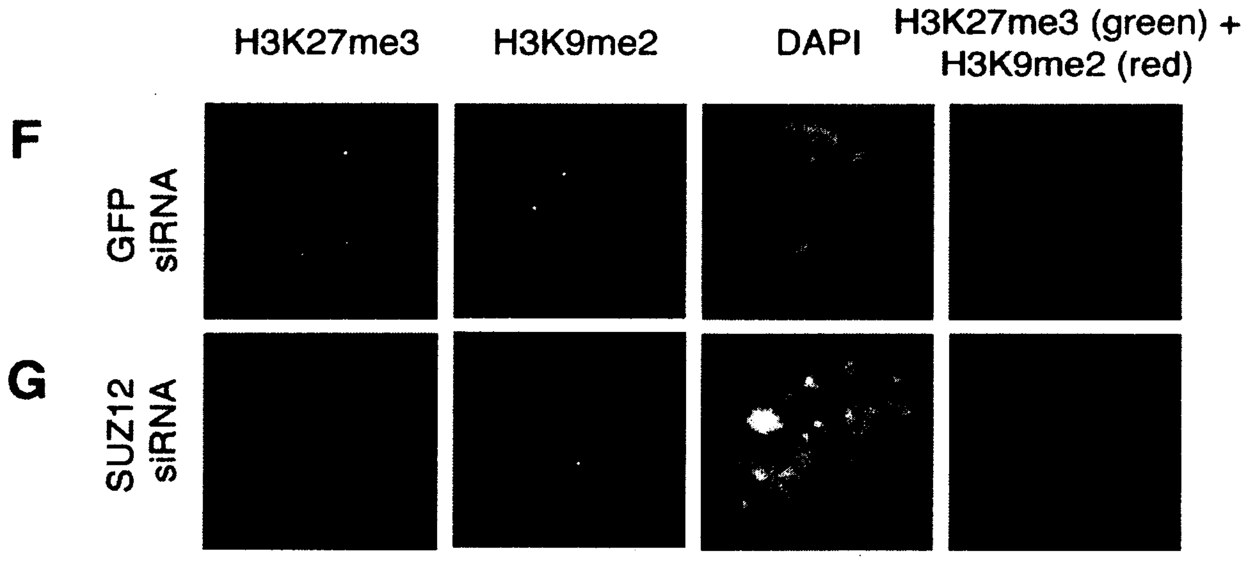

Figure 2. Distribution of H3K9me3 and H3K9me2 in SUZ12 knockdown cells. **A–D**: Immunolocalization of SUZ12 (first column) and H3K9me3 (second column) in IMR90 cells treated with GFP siRNA (**A,C**) or SUZ12 siRNA (**B,D**). Nuclei are stained with DAPI (third column) and the merged image (fourth column) consists of SUZ12 (red) and H3K9me3 (green). **E**: Western analysis of SUZ12, H3K27me3, H3K9me3, histone H3 and actin levels in mock, SUZ12 siRNA, and GFP siRNA transfected IMR90 cells. **F,G**: Immunostaining for H3K27me3 (first column) and H3K9me2 (second column) in IMR90 cells treated with GFP siRNAs (**F**) or SUZ12 siRNAs (**G**). Nuclei are stained with DAPI (third column) and the merged panel (fourth column) consists of H3K27me3 (green) and H3K9me2 (red).

50% of the population (de la Cruz *et al.* 2005). H3K9me3 levels were markedly reduced in 92% of the cells with no detectable SUZ12, but not in cells that retained some SUZ12 staining (Figure 2B and D, $n > 100$). This phenotype was also observed when SUZ12 siRNA was performed in two additional primary human cell lines, WI38 and HEL 299 cells (data not shown). Western blot analyses of knockdown IMR90 cells showed a 2–3-fold decrease of H3K9me3 when compared to mock transfected and GFP siRNA transfected cells (Figure 2E). The 2-fold difference observed by Western blotting can be explained by our immunofluorescence studies, which reveal that about half of the total cell population showed lowered levels of H3K9me3. As expected, knockdown of SUZ12 in IMR90 cells resulted in a 5-fold reduction in H3K27me3 as assayed by Western blotting (Figure 2E) and immunostaining (Figure 2D and E; de la Cruz *et al.* 2005).

To determine if the SUZ12 knockdown phenotype was specific for tri-methylation of H3-K9, we co-stained control cells and SUZ12 siRNA-treated cells for H3K27me3, to identify cells with significant depletion of SUZ12, and for di-methylated H3-K9 (H3K9me2). There was no discernible difference in the levels of H3K9me2 between GFP siRNA and SUZ12 siRNA transfected cells as assayed by immunofluorescence (Figures 2F and G). These results indicate that SUZ12 regulates levels of H3K9me3 but not H3K9me2.

Knockdown of EZH2 results in loss of H3K27me3 but not H3K9me3

In addition to H3K27me3 activity, EZH2/EED complexes have limited H3-K9 HMTase activity *in vitro* (Kuzmichev *et al.* 2002). To determine if the H3K9me3 phenotype of SUZ12 knockdown cells was due to abrogation of EZH2/EED H3-K9 HMTase activity, we performed EZH2 knockdown experiments. EZH2 knockdown cells were stained using antibodies against H3K27me3 and H3K9me3 to examine levels and distribution of these chromatin marks. GFP siRNA transfected IMR90 cells exhibit a very low level of EZH2 present in dim speckles (Figure 3A). After 6 days of incubation with EZH2 siRNAs, 44% of cells exhibited a loss of EZH2 accompanied by a drastic reduction of H3K27me3

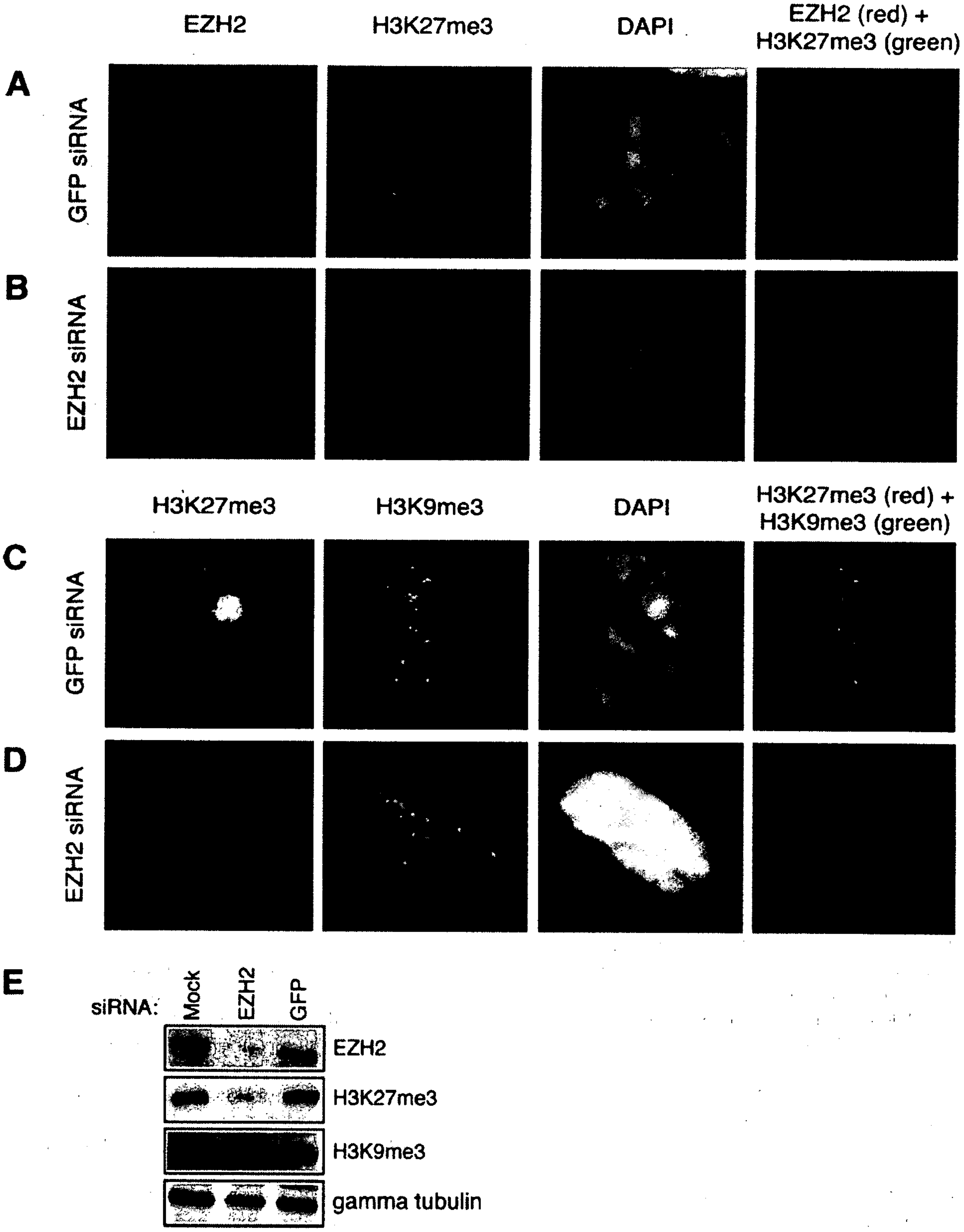
EZH2
H3K27me3
DAPI
EZH2 (red) + H3K27me3 (green)
A
GFP siRNA
B
EZH2 siRNA
H3K27me3
H3K9me3
DAPI
H3K27me3 (red) + H3K9me3 (green)
C
GFP siRNA
D
EZH2 siRNA
E
siRNA:
Mock
EZH2
GFP
EZH2
H3K27me3
H3K9me3
gamma tubulin

(Figure 3B). Cells treated with EZH2 siRNA were co-stained for H3K27me3 and H3K9me3 (Figure 3C and D). In contrast to SUZ12 knockdown, loss of EZH2 caused a reduction of H3K27me3 staining but did not affect levels of H3K9me3 (Figure 3C and D). Western blot analysis of EZH2 knockdown cells corroborated the immunofluorescence results: levels of H3K27me3 were reduced 3-fold in EZH2 knockdown cells as compared to mock and GFP siRNA transfected cells, whereas H3K9me3 levels were reduced by only 0.2-fold (Figure 3E). We conclude that the H3K9me3 phenotype observed in SUZ12 knockdown cells is not linked to the reduction in the overall amount of H3K27me3. In addition, these experiments indicate that the SUZ12 siRNA H3K9me3 phenotype is due to the loss of a SUZ12 function that is independent of SUZ12's role in EZH2-directed HMTase activity.

HP1α distribution is altered in SUZ12 knockdown cells

HP1 localization is regulated by H3-K9 methylation (Bannister *et al.* 2001, Maison *et al.* 2002, Pal-Bhadra *et al.* 2004, Peters *et al.* 2001, Rice *et al.* 2003, Yamamoto *et al.* 2004), suggesting that localization of HP1α may be affected in SUZ12 knockdown cells with lowered levels of H3K9me3. In GFP siRNA transfected IMR90 cells there were two predominant patterns of H3K9me3/HP1α localization (Figure 4A, B), consistent with dynamic localization of HP1α on constitutive heterochromatin (Cheutin *et al.* 2003, Festenstein *et al.* 2003, Hayakawa *et al.* 2003). In 80% of cells, H3K9me3 exhibited strong foci of enrichment that overlapped with toroidal HP1α staining (Figure 4A) indicative of constitutive heterochromatin (Minc *et al.* 1999, Nielsen *et al.* 2001). These cells also showed a large number of fine speckles of HP1α that did not overlap with H3K9me3. The remaining 20% of GFP siRNA transfected cells displayed relatively uniform distribution of slightly larger HP1α speckles, and these cells always displayed a diffuse pattern of H3K9me3 speckles, with no significant overlap between H3K9me3 and HP1α (Figure 4B). When SUZ12 siRNA cells were subjected to standard immunostaining procedures, which included a Triton X-100 detergent extraction, cells exhibiting low levels of H3K9me3 displayed a very low level of diffusely distributed HP1α in 87% of cells (Figure 4C).

HP1α is present in Triton X-100 soluble and insoluble pools, and the insoluble pools contain HP1α that is bound to heterochromatin (Maison *et al.* 2002, Taddei *et al.* 2001). To test if SUZ12 knockdown affects total levels of HP1α or causes redistribution of HP1α from insoluble heterochromatin-associated pools to soluble, non-heterochromatin-associated pools, we performed immunostaining for H3K9me3 and HP1α on SUZ12 knockdown cells that had not been Triton X-100 extracted prior to fixation (Figure 4D). Non-Triton X-100 extracted cells with lowered levels of H3K9me3 contained diffusely distributed HP1α at levels comparable to GFP siRNA-treated cells, but never had HP1α toroids. In addition, Western blotting of SU(Z)12 siRNA-treated cells that were not extracted by Triton X-100 showed that total levels of HP1α protein are not severely affected in SUZ12 knockdown cells (Figure 4E). These results suggest that SUZ12 knockdown results in redistribution of HP1α from heterochromatin-associated pools to soluble pools.

Enrichment of HP1α on pericentric heterochromatin requires concomitant accumulation of H3K9me3, and both of these marks are required for centromere function and normal chromosome segregation (Peters *et al.* 2001, Taddei *et al.* 2001). Given that levels of H3K9me3 are reduced on pericentric heterochromatin in a significant fraction of SUZ12 knockdown cells, we expected that knockdown cells would exhibit defects in chromosome segregation. A common marker of chromosome instability is the appearance of micronuclei and chromatin bridges, which form when lagging chromosomes become surrounded by a nuclear envelope (Hoffelder *et al.* 2004). Consistent with a defect in chromosome segregation, there was a 3-fold increase in the proportion of cells containing micronuclei and chromatin bridges in SUZ12 knockdown cells com-

Figure 3. EZH2 knockdown results in depletion of H3K27me3 but not H3K9me3. **A,B**: Immunostaining for EZH2 (first column) and H3K27me3 (second column) in IMR90 cells treated with GFP siRNAs (**A**) or EZH2 siRNAs (**B**). Nuclei are stained with DAPI (third column) and the merged panel (fourth column) consists of EZH2 (red) and H3K27me3 (green). **C,D**: Immunostaining for H3K27me3 (first column) and H3K9me3 (second column) in IMR90 cells treated with GFP siRNAs (**C**) or EZH2 siRNAs (**D**). Nuclei are stained with DAPI (third column) and the merged panel (fourth column) consists of H3K27me3 (red) and H3K9me3 (green). **E**: Western blotting for EZH2, H3K27me3, H3K9me3, and gamma tubulin in IMR90 cells transfected with no siRNA, SUZ12 siRNA, or GFP siRNA.

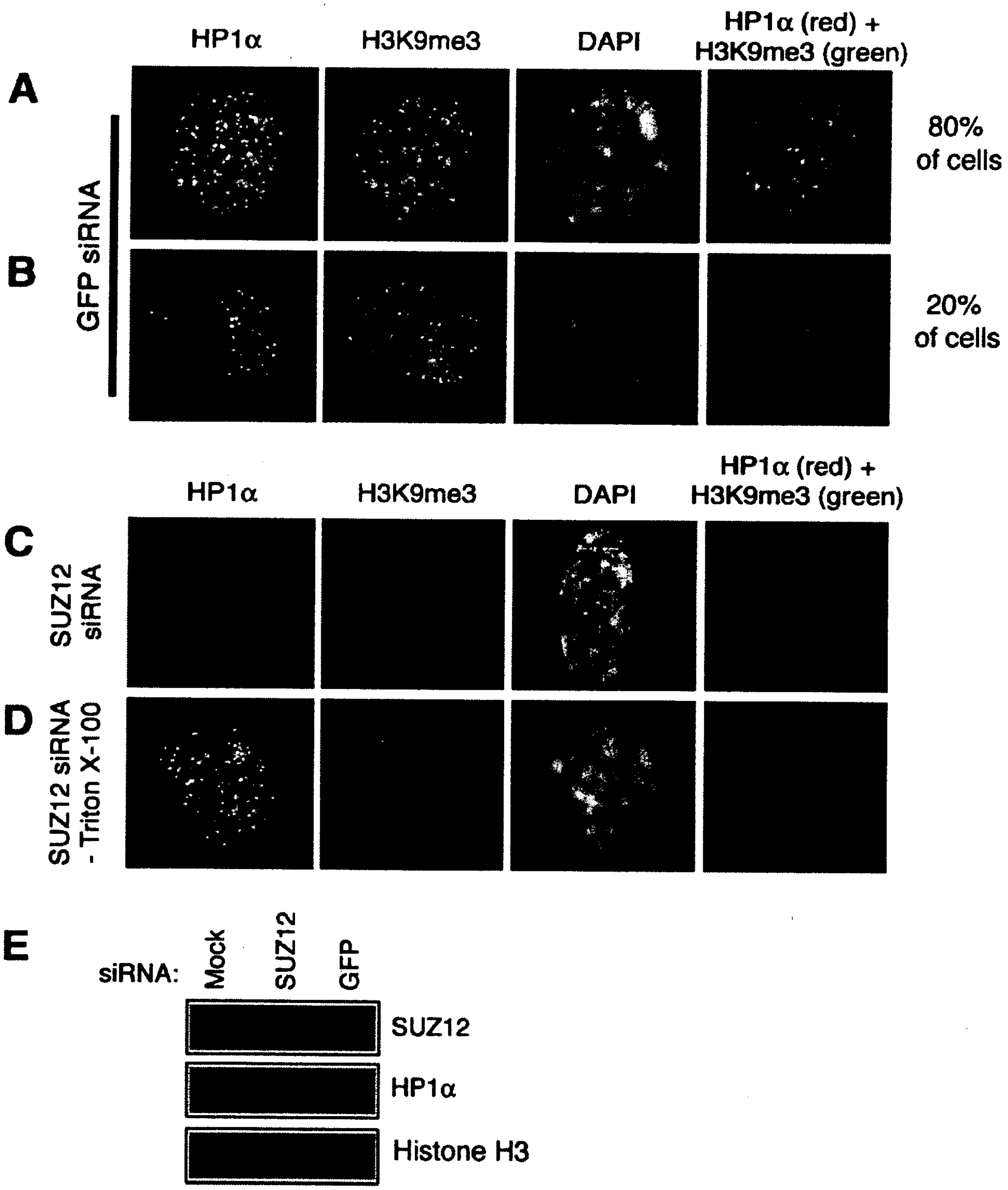
HP1α
H3K9me3
DAPI
HP1α (red) + H3K9me3 (green)
A
B
GFP siRNA
80% of cells
20% of cells
HP1α
H3K9me3
DAPI
HP1α (red) + H3K9me3 (green)
C
SUZ12 siRNA
D
SUZ12 siRNA - Triton X-100
E
siRNA:
Mock
SUZ12
GFP
SUZ12
HP1α
Histone H3

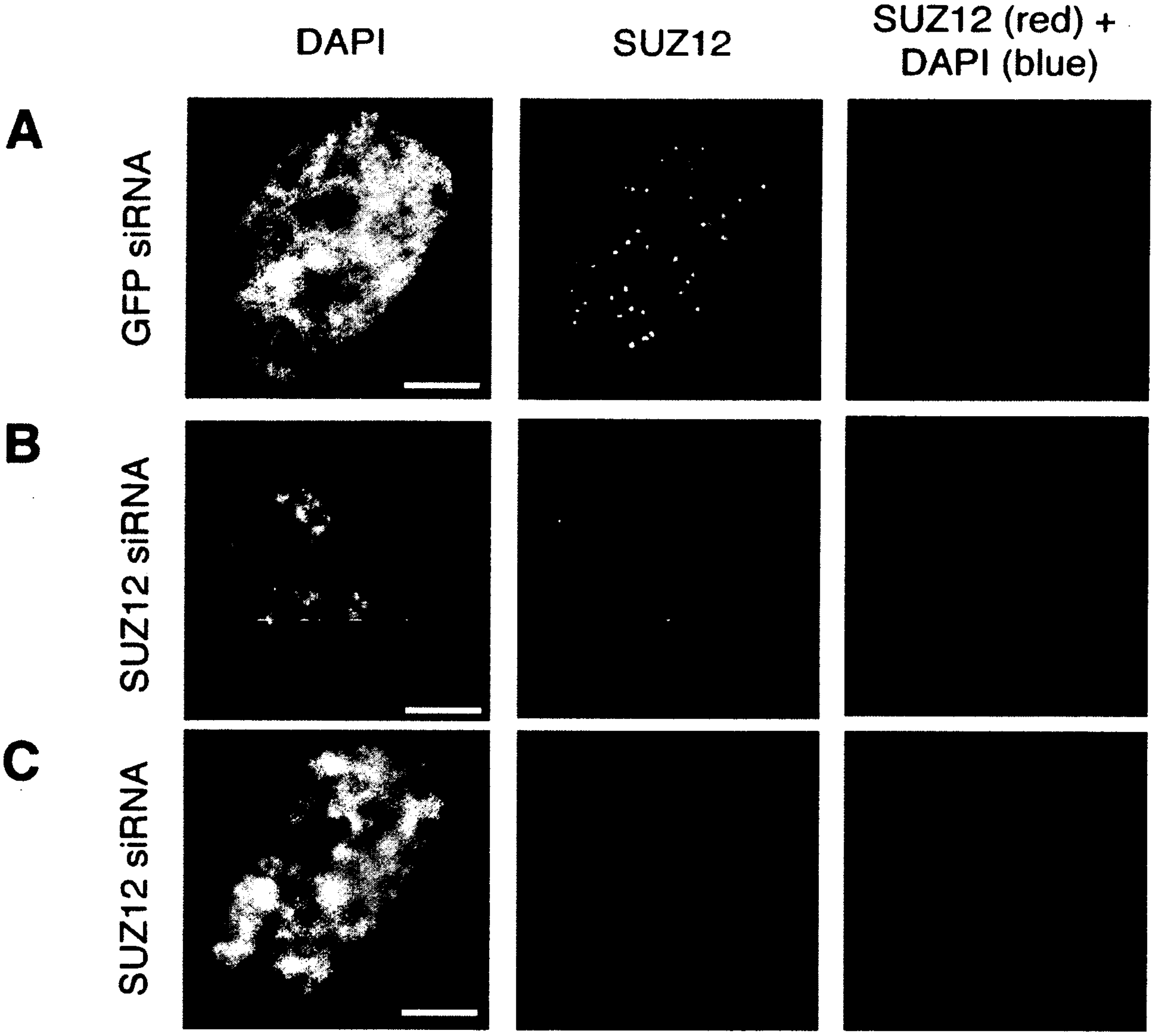

Figure 5. Increase in micronuclei and chromatin bridges in SUZ12 knockdown cells. A–C: Immunostaining for SUZ12 (second column) in IMR90 cells treated with GFP siRNAs (A) or SUZ12 siRNAs (B,C) Nuclei are stained with DAPI (first column) and the merged panel (third column) consists of SUZ12 (red) and DAPI (blue). **B**: A SUZ12 knockdown cell with micronuclei. C: A SUZ12 knockdown cell exhibiting a chromatin bridge. Scale bar=5 μm.

Figure 4. Distribution of HP1α in SUZ12 knockdown cells. **A,B**: Immunolocalization of HP1α (first column) and H3K9me3 (second column) in GFP siRNA treated IMR90 cells. Nuclei are stained with DAPI (third column) and the merged image (fourth column) consists of HP1α (red) and H3K9me3 (green). HP1α and H3K9me3 show two patterns of distribution: HP1α is present in many speckles, which in some instances are organized into toroids that overlap with H3K9me3 toroids (A), and HP1α and H3K9me3 show many speckles with no toroids and no significant amount of overlap (**B**). **C,D**: Immunolocalization of HP1α (first column) and H3K9me3 (second column) in SUZ12 siRNA treated IMR90 cells. In SUZ12 siRNA-treated cells that show little or no detectable H3K9me3, HP1α is also not detectable when cells are extracted with Triton X-100 (C), but remains detectable in cells that were not Triton X-100 extracted (**D**). E: Western blotting for SUZ12, HP1α, and histone H3 in non-Triton X-100 extracted IMR90 cells transfected with no siRNA, SUZ12 siRNA, or GFP siRNA.